Solids mixing and segregation in binary fluidized beds - Defining spatiotemporal patterns using a novel magnetic solids tracing technique

Downloaded from: https://research.chalmers.se, 2026-06-13 12:46 UTC

Citation for the original published paper (version of record):
Siddiqui, A., Kohler, A., Guio Perez, D. et al (2026). Solids mixing and segregation in binary fluidized beds - Defining spatiotemporal patterns using a novel magnetic solids tracing technique. Powder Technology, 480. http://dx.doi.org/10.1016/j.powtec.2026.122561

N.B. When citing this work, cite the original published paper.

research.chalmers.se offers the possibility of retrieving research publications produced at Chalmers University of Technology. It covers all kind of research output: articles, dissertations, conference papers, reports etc. since 2004. research.chalmers.se is administrated and maintained by Chalmers Library

(article starts on next page)

Powder Technology 480 (2026) 122561

Contents lists available at ScienceDirect

Powder Technology

journal homepage: www.journals.elsevier.com/powder-technology

Solids mixing and segregation in binary fluidized beds - Defining spatiotemporal patterns using a novel magnetic solids tracing technique☆

Azka Rizwana Siddiqui [a,*], Anna Köhler [b], Diana Carolina Guío-Pérez [a], David Pallarès [a]

[a] Division of Energy Technology, Department of Space, Earth and Environment, Chalmers University of Technology, SE-412 96 Gothenburg, Sweden
[b] BioShare AB, Karlstad, Sweden

HIGHLIGHTS

- Novel impedance coil system enables spatiotemporal mapping of solids concentration.
- Mixing metrics mapped for hot industrial-scale conditions.
- Higher fluidization velocity and bed height boost mixing index and rates.
- Trends align with cold condition studies, however critical loading values differ.
- Mixing of solids occurs at lower frequency than bubble dynamics.

GRAPHICAL ABSTRACT

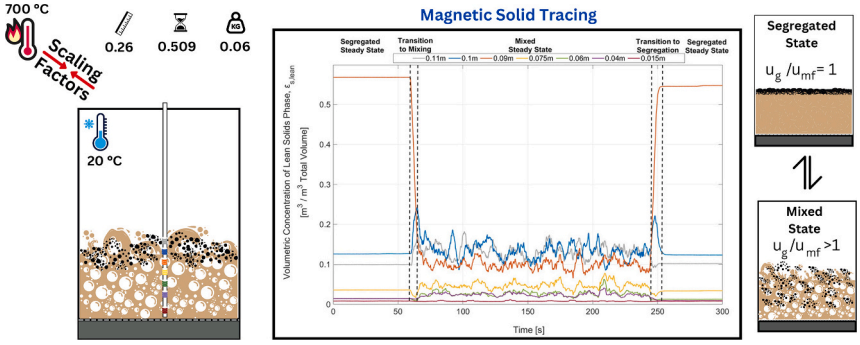

ARTICLE INFO

Keywords:
Binary fluidized beds
Solids mixing
Solids segregation
Magnetic solids tracing
Mixing index
Mixing rates

ABSTRACT

This study investigates the vertical mixing and segregation patterns of a lean solids phase in a bubbling fluidized bed. A novel measurement method is introduced that allows for online acquisition of the vertical distribution of the lean solids phase using magnetic solids tracing (MST) coils arranged along a pin-probe. This method enables spatiotemporal profiling of the lean solids phase, based on which the mixing indices and transitional velocities between the mixing and segregation states can be calculated, as well as the concentrations in the frequency domain. Experiments are conducted under fluid-dynamically downscaled conditions resembling a large-scale (1.33 m^2 in cross-section) unit fluidizing sand (Geldart B) and biomass particles (lean solids phase) at 700 °C, typical of thermochemical conversion processes. The impacts of fluidization velocity, bed height, and lean phase loading are analyzed.

Increasing the fluidization velocity enhanced mixing, whereas lean phase loadings above ~10%$_{vol}$ led to surface layering, which dampened the bubble eruptions and reduced particle mobility. Taller beds promoted deeper penetration of the lean phase into the dense bed and reduced stratification, while shallow beds and high loadings favored segregation, highlighting the critical roles of these parameters in the mixing behavior. Transitions between the segregated and mixed states were modulated by the bed height and fluidization velocity, suggesting a relationship with the characteristics of the bubble phase. However, mixing of the lean phase

☆ This article is part of a Special issue entitled: 'FBC25' published in Powder Technology.

* Corresponding author.
E-mail address: azkar@chalmers.se (A.R. Siddiqui).

https://doi.org/10.1016/j.powtec.2026.122561
Received 14 November 2025; Received in revised form 6 April 2026; Accepted 13 April 2026
Available online 15 April 2026
0032-5910/© 2026 The Authors. Published by Elsevier B.V. This is an open access article under the CC BY license (http://creativecommons.org/licenses/by/4.0/).

occurred at a lower characteristic frequency compared to the dominant frequency of the bed dynamics, indicating that although bubbles induce solids mixing, not all bubbles contribute effectively.

Nomenclature

Symbols

d_p	Diameter of particle [mm]
FN	Fluidization number [−]
f	Frequency [Hz]
g	Gravitational constant, 9.81 [m/s^2]
$H_{b,0}$	Static bed height [m]
H_b	Expanded bed height [m]
L*	Characteristic length [m]
M	Mixing Index [−]
m	Mass [kg]
P	Pressure [Pa]
ΔP	Pressure drop [Pa]
T	Temperature [°C]
τ_{mix}*	Characteristic time of mixing [s]
τ_{seg}*	Characteristic time of segregation [s]
u_g	Fluidization velocity [m/s]
u_{mf}	Minimum fluidization velocity [m/s]
ε_g	Bed voidage [−]
ε_s	Volumetric concentration of solids [−]
Φ	Sphericity [−]
ϰ	Loading of solids phase $\%_{vol}$]
ρ	Density [kg/m^3]
σ	Variance [−]

Subscripts

bulk	Bulk solids phase
g	Gas phase
lean	Lean solids phase
s	Solids

1. Introduction

Binary fluidized beds – which involve two solids phases that differ significantly in terms of density, size and/or shape – are present in many industrial sectors, i.e., thermochemical conversion, mineral processing, and the food and pharmaceutical industries. The solids phase that makes up the largest fraction of the bed, often referred to as the *bulk solids*, facilitates heat transfer, provides a catalytic surface and/or enhances the mixing of the secondary solids phase. The latter, present in lower concentrations and often referred to as the *lean solids phase*, is typically the phase that undergoes the main physical and/or chemical conversion in the process.

In the absence of bubbles, the differences in particle properties inherently drive the vertical segregation of gas-solids suspensions. The presence of a bubble flow affects this segregating tendency by continuously altering the local voidage and creating gas and solids flows, and thus the drag forces that promote both vertical and lateral mixing of both solids phases [1]. This feature is key to the design and operation of binary beds, for which it is crucial to be able to predict how the operating conditions will impact the mixing of the solids phases and how the resulting solids distribution will influence mass and heat transfer. However, this is a challenging task, given the differences in physical properties between the two solids phases; the competing buoyancy and drag forces develop into strong dynamics and mixing and segregation behaviors that are difficult to measure or predict [1–4].

This work focuses on a situation that is commonly encountered in industrial applications: a binary bed in which the solids lean phase is coarser and lighter than the bulk solids phase. This occurs, for example, in the thermochemical conversion of solid fuels, where the lean solids phase consists of solid fuel particles and is much larger and lighter (typically 1–50 mm, 50–900 kg/m^3) than the sand-like bulk solids (typically <0.3 mm, 1500–3000 kg/m^3).

The current literature offers relevant information on the mixing and segregation behaviors of binary beds. Experimental studies on solids mixing and segregation in binary beds, particularly those involving coarser and/or lighter lean solids, are summarized in Table 1. The focus is on research published after Year 2000, as advances in measurement techniques since then have improved our ability to gain insights into the mixing phenomena.

Notably, the vast majority of the studies reported in literature have relied on experiments conducted in small beds (<0.2 m in diameter) under ambient conditions, primarily due to the technical challenges that high temperatures pose for measurement techniques. Nevertheless, a few studies have provided insights into solids mixing and segregation in hot large-scale binary beds using camera imaging [30,31], despite the limitations related to accuracy and gross assumptions and a lack of penetration into the dense bed.

While experimental studies conducted under ambient conditions disregard the temperature effect, they can exploit a broader range of measurement techniques, facilitating more-accurate assessments and, thus, providing more-detailed insights into the solids mixing phenomenon. Simple visualization has often been employed to assess mixing and segregation quality [17,27]. The frozen bed method makes it possible to extract a concentration profile, although it fails to capture the real-time dynamics of mixing and segregation [6–9,12,14,15,24]. Optical imaging techniques can be used in cold pseudo-2D units, offering time resolution and insights into the dense bed, although they suffer from a not-yet-quantified impact of the restricted geometry [13,20,26]. Particle tracking methods offer detailed information about the dynamics of solids mixing by following individual particles within the bed [11,15,16,28], with the main challenge being the design of tracer particles of adequate size and density. In many instances, the currently available techniques for particle tracking are limited to a single particle, thereby missing out on the influence of collisions among particles within the lean solids phase. This problem can be addressed through the use of dummy tracer particles [5], although the challenge remains in relation to finding tracer and dummy particles with matching properties. While particle tracking techniques can provide detailed 3D trajectory and mixing rates in binary beds, they primarily yield trajectory-resolved data. To obtain concentration fields with particle tracking, measurements must be collected over long durations and averaged in time, which limits the ability to capture instantaneous concentration fluctuations. Solids tracing techniques represent an alternative approach in which time-resolved concentration data from a solids batch can be used to derive mixing parameters [18]. Existing tracing methods (chemical or color tracing) [32–34] typically provide either spatial or temporal resolution, but rarely both. One such tracing technique, magnetic solids tracing (MST), exploits ferromagnetic tracer particles, which are generally safe to handle, less toxic than alternative radioactive tracers, and available with a relatively wide range of physical properties [35,36]. Since its development, MST has been exploited to quantify

Table 1
Summary of experimental studies and their key findings regarding mixing and segregation in binary fluidized beds (references are listed chronologically).

Reference	Aim of work	Cross-section geometry	Gas and Solids Phases		Operating Conditions		Methodology	Summary
Wirsum et al. [5]	Investigation of the motion and time-dependent vertical distribution of large, light lean solids phase particles.	Rectangular, 0.45 m × 0.45 m	**Bulk Solids**	Quartz sand	T_{bed}	30°–50 °C	Electromagnetic particle detection using dummy tracer particles to ensure lean-particle interactions. Particle trajectories were tracked to calculate residence time, expanded bed height, and mixing indices.	Smaller and heavier lean solids mixed better.
			$\rho_{s,bulk}$	2600 kg/m^3	H/D	1.1		
			d_p	0.41 / 0.91 mm	$H_{b,0}$	0.5 m		
			Geldart Type	B / D	u_g	0.2 / 1.1 m/s		
			Lean Solids	Spheres made of wood and plastic	Lean Fraction	1.89 / 7.02%$_{vol}$		Coarse lean solids phase segregated at bed surface.
			$\rho_{s,lean}$	440 / 680 / 730 / 1130 / 1420 kg/m^3				Mixing improved by finer bulk solids and higher fluidization velocity.
			d_p	20 / 30 / 40 mm				
			Fluidizing Gas	Air				
Olivieri et al. [6]	Study of the extent and dynamics of solids segregation in binary mixtures.	Cylindrical, 0.12 m ID	**Solid Phases**	Silica sand & silica gel / Silica sand & polypropylene / Glass beads & silica sand	T_{bed}	30°–50 °C	Pressure transducers and frozen bed method used to measure vertical concentration profiles, mixing index, and fluidization regimes.	Minimum fluidization velocity of an individual component does not accurately predict segregation patterns.
					H/D	1.1 / 1.2		
					$H_{b,0}$	0.132 / 0.144 m		
					u_g	1.73–3.5 u_{mf}		
			ρ_s	2600 & 600 / 2600 & 900 / 2540 & 2600 kg/m^3	Solids Fraction	10–80%$_{vol}$		
			d_p	0.125 & 0.375 / 0.5 & 0.5 / 0.5 & 0.125 mm				More research is needed to predict the fluidization velocity needed for uniform mixing.
			Φ_s	~1				
			Geldart Type	B & A-B / B & B / B & B				
			Fluidizing Gas	Air				
Zhang et al. [7]	Investigation of the mixing and segregation behaviors of biomass particles in biomass–sand mixtures.	Rectangular, 0.4 m × 0.4 m	**Bulk Solids**	Quartz sand	T_{bed}	Ambient	Frozen bed technique used to obtain vertical concentration profiles and mixing index, complemented by digital camera imaging to visualize flow patterns.	Mixing dominates up to a critical fluidization velocity, after which segregation starts to dominate once again.
					H/D	0.75		
			$\rho_{s,bulk}$	2560 kg/m^3	$H_{b,0}$	0.3 m		
			d_p	0.5 mm	u_g	1–10 u_{mf}		
			Φ_s	~1	Lean Fraction	1 / 2 / 3%$_{wt}$		
			Geldart Type	B				
			Lean Solids	Biomass (Cotton stalk)				
			$\rho_{s,lean}$	385.3 kg/m^3				
			d_p	50 × 5 mm				
			Φ_{lean}	Cylindrical				
			Fluidizing Gas	N/A				
Jang et al. [8]	Investigation of the mixing and segregation behaviors and residence times of binary fluidized beds with solids throughput.	Cylindrical, 0.109 m ID	**Bulk Solids**	Sand	H/D	1	Frozen bed technique combined with use of pressure transducers to study particle behavior, concentration distribution and residence time.	Bulk phase fluidization mobility is higher with lower loadings of lean phase.
					$H_{b,0}$	0.109 m		
			$\rho_{s,bulk}$	2620 kg/m^3	u_g	1.73–3.5 u_{mf}		
			d_p	0.715 mm	Lean Fraction	0.3–1.0%$_{vol}$		Lean phase mobility remains constant for varying fluidization velocities.
			Lean Solids	Polymethylmethacrylate				
			$\rho_{s,lean}$	1190 kg/m^3				Larger particle size ratios result in greater residence time deviations between particle types.
			d_p	1.545 / 0.715 / 0.359 mm				
			Fluidizing Gas	Air				Solid movement quantified by residence time distribution is a better indicator of mixing than axial concentration distribution alone.
Rao et al. [9]	Investigation of the mixing and segregation behaviors of binary mixtures under steady state conditions.	Cylindrical, 0.09 m ID	**Bulk Solids**	Sand	T_{bed}	$T_{Ambient}$	Frozen bed technique combined with pressure transducers to obtain concentration and bed expansion	Size of bulk solids impacts the fluidization and mixing behaviors of binary beds, with prominent effects
					H/D	0.67		
			$\rho_{s,bulk}$	2520 kg/m^3	$H_{b,0}$	0.06 m (0.03 m bulk solids phase)		
			d_p	0.93 / 0.66 / 0.4 mm				

(*continued on next page*)

Table 1 (*continued*)

Reference	Aim of work	Cross-section geometry	Gas and Solids Phases		Operating Conditions		Methodology	Summary
			Lean Solids	Rice husk / Sawdust / Groundnut shell	u_g	0.48–0.65 m/s		observed for mixtures with a fine lean solids phase.
			$\rho_{s,lean}$	589 / 716 / 680 kg/m^3	Lean	1:13 / 1:5 / 1:12		
			d_p	2.094 / 0.578 / 8.78 mm	Fraction	(6.7 / 15.44 / 7.19%$_{wt}$)		
			Fluidizing Gas	Air				Higher gas velocity enhances mixing.
Upadhyay et al. [10]	Investigation of mixing and flow behavior of binary mixture.	Cylindrical, 0.115 m ID	**Solid Phases**	Glass beads / Sago Beads	T_{bed}	$T_{Ambient}$	Radioactive Particle Tracking (RPT) to obtain velocity fields and Dual-Source Densitometry (DSD) to measure solids volume fractions	Particle collisions drive movement in binary beds.
					u_g	0.9–1.3 m/s		
			ρ_s	2600 / 1350 kg/m^3	Solids	0–100%$_{wt}$		
			d_p	1.5 / 1.5 mm	Fraction			
			Fluidizing Gas	Air				Light particles fluidize heavy ones below their normal fluidization velocity.
								Mixtures retain concentration gradients even at high gas velocities.
Halow et al. [11]	A detailed spatiotemporal understanding of the mixing behaviors of fuel particles, to support the development of statistical models.	Cylindrical, 0.055 m ID	**Bulk Solids**	Glass beads	T_{bed}	$T_{Ambient}$	Magnetic particle tracking in a bed with dummy lean particles, while a Weibull distribution aids statistical modeling.	Particle behavior transitions from segregated to well-mixed as density approaches that of the bed material.
					H/D	1		
			$\rho_{s,bulk}$	2500 kg/m^3	$H_{b,0}$	0.055 m		
			d_p	0.177–0.25 mm	u_g	1–6 u_{mf}		
			Φ_s	~1	Lean	0–10%$_{wt}$		
			Lean Solids	Magnetically tagged wood particles	Fraction			Temporal autocorrelations reveal dominant bed circulation timescales (one rise-sink cycle driven by bubbles) that vary with fluidization velocity.
			$\rho_{s,lean}$	550–1200 kg/m^3				
			d_p	3–4 mm				
			Fluidizing Gas	Air				
Zhang et al. [12]	Investigation of the hydrodynamics of binary fluidized beds and gas jets at high loadings for the lean solids phase.	Rectangular, 0.3 m × 0.025 m	**Bulk Solids**	Resin	T_{bed}	$T_{Ambient}$	Frozen bed experiments combined with high-speed digital imaging are used to investigate the mixing index and minimum fluidization velocity.	Bulk solids phase improves fluidization quality in comparison to system with exclusively lean solids phase.
			$\rho_{s,bulk}$	1148 kg/m^3	u_g	0.37–1.48 m/s		
			d_p	0.75 mm	u_{jet}	50–90 u_{mf}		
			Lean Solids	Tobacco stem	Lean	0–20%$_{wt}$		Lean fraction <7%$_{wt}$ is optimal for maximal mixing.
			$\rho_{s,lean}$	850 kg/m^3	Fraction			
			d_p	17.5 mm				Jet gas aids mixing and is required for effective mixing of higher lean fractions.
			Fluidizing Gas	Air				
Olaofe et al. [13]	Investigation of segregation patterns in binary and ternary mixtures.	Pseudo 2D, 0.3 m × 0.015 m	**Solid Phases**	Matted glass particles (three-colored)	T_{bed}	$T_{Ambient}$	Digital camera imaging used to quantify a segregation index.	Binary mixtures segregate near minimum fluidization velocity.
					H/D	1		
			ρ_s	~2550 kg/m^3	$H_{b,0}$	0.3 m		
			d_p	1.5–3.5 mm	u_g	1.1–1.5 u_{mf}		Ternary mixtures mix well at gas velocities that are even lower than the minimum fluidization velocity of the larger particles.
			Fluidizing Gas	Air	Solids Fraction	25–75%$_{wt}$		
Cluet et al. [14]	Investigation of the axial segregation of the lean solids phase in a larger bed (minimized wall effects).	Cylindrical, 0.242 m ID	**Bulk Solids**	Non-ferrous olivine	T_{bed}	$T_{Ambient}$	Pressure transducers and in-bed sampling are used to obtain concentration profiles and mixing indices.	Coarser bulk solids yield variable bed voidage along the bed height.
					H/D	1.1 / 1.6		
			$\rho_{s,bulk}$	3250 kg/m^3	$H_{b,0}$	0.265 / 0.391 m		
			d_p	0.378 / 0.237 mm	u_g	1.736 / 2.78 m/s		
			Φ_s	0.82 / 0.78	Lean	30 / 50 / 70%$_{wt}$		For fine bulk solids, the voidage decreased in the upper part of the bed.
			Geldart Type	B	Fraction			
			Lean Solids	Wood (Beech / Balsa)				
			$\rho_{s,lean}$	685 / 159 kg/m^3				
			d_p	80 × 250 / 55 × 40 × 570 / 55 × 40 × 570 / 20 × 40 × 295 mm				Mixing increases with denser and less-spherical lean solids.
			Φ_{lean}	0.77 / 0.5				
			Fluidizing Gas	Air				50%–80% of lean solids phase stays in bed, while remainder segregates at the bed surface.

(*continued on next page*)

Table 1 (*continued*)

Reference	Aim of work	Cross-section geometry	Gas and Solids Phases		Operating Conditions		Methodology	Summary
Fotovat et al. [15]	Investigation of the segregation behavior of the lean solids phase.	Cylindrical, 0.152 / 0.192 m ID	**Bulk Solids**	Silica sand / Glass beads	T_{bed}	$T_{Ambient}$	Radioactive particle tracking, fiber-optic sensors, and frozen bed techniques used to study particle motion, bubbling behavior, and solids mixing, to quantify axial distribution, bubble size, mixing index, bubble rise velocity, and lean solids circulation, and to couple experimental results with a 3-D Eulerian–Eulerian CFD approach for detailed analysis.	The shape of the lean solids phase affects fluidization by influencing bubble formation and, consequently, the circulation of solids in the bed. The frozen bed method becomes unreliable at high bed expansion, attained at, for example, high gas velocity or low lean fraction.
					H/D	1.5		
			$\rho_{s,bulk}$	2650 / 2500 kg/m^3	$H_{b,0}$	0.228 / 0.288 m		
			d_p	0.38 / 500 mm	u_g	2 / 3.6 & 4 u_{mf}		
			Φ_s	~1	Lean Fraction	2 / 8 / 16%$_{wt}$		
			Lean Solids	Biomass				
			$\rho_{s,lean}$	824 / 644 kg/m^3				
			d_p	12.70 × 6.35 mm / 9.53 mm				
			Φ_{lean}	0.874 / 1				
			Fluidizing Gas	Air				
Köhler et al. [16]	Study of the axial mixing of the lean solids phase at different stages of conversion under experimental conditions representative of large-scale industrial applications.	Cold flow model, 0.17 m × 0.17 m (*upscaled model, 0.74 m × 0.74 m*)	**Bulk Solids**	Bronze powder (*Silica sand*)	T_{bed}	20 °C (*800 °C*)	Magnetic Particle Tracking to study axial segregation, mixing index, and circulation of lean solids.	Larger bubbles enhance the vertical mixing of lean solids. Three regimes are identified as the fluidization velocity increases: segregated; transition; and full mixing. The regime shifts depend on the bed height and the density of the lean solids. The distributor plate with greater pressure drop promotes stronger flotsam behavior of the lean solids phase.
					H/D	0.25 / 0.41		
			$\rho_{s,bulk}$	8900 (*2600*) kg/m^3	$H_{b,0}$	0.18 / 0.305 m		
			d_p	0.60 (*0.25*) mm	u_g	0.013–0.53 m/s		
			Lean Solids	Synthetic tracer (*Biomass*)	$\Delta P_{distributor}$	131.23 u_0^2 / 51.76 u_0^2 kPa		
			$\rho_{s,lean}$	1280–4500 (*350–1230*) kg/m^3				
			d_p	10 (*44*) mm				
			Φ_{lean}	1				
			Fluidizing Gas	Ambient air (*Air*)				
Brachi et al. [17]	Investigation of the fluidization and segregation of polydisperse binary mixtures.	Cylindrical, 0.1 m ID	**Bulk Solids Phase**	Quartz sand / Silica sand / Commercial γ-alumina powder / Commercial γ-alumina spheres	T_{bed}	$T_{Ambient}$	Piezo-resistive pressure sensors and visualization used to study fluidization behavior and segregation at bed surface.	Density difference prevails over size difference in segregation. Small dense (Geldart A) bulk particles allow lean solid phase to act as jetsam, whereas large dense (Geldart B) bulk particles yield a flotsam lean phase.
					H/D	2.2		
					$H_{b,0}$	~0.22 ± 0.02 m		
					u_g	u_{mf} - $u_{slugging}$		
			$\rho_{s,bulk}$	2813.5 & 2650.6 / 3986.9 & 3986.9 kg/m^3	Lean Fraction	0–5 / 0–20 / 0–42 / 0–38%$_{vol}$		
			d_p	0.1–0.25 & 0.15–0.4 / 0.05–0.25 & 0.2–0.4 mm				
			Geldart Type	B / B / A / B				
			Lean Solids Phase	Orange peels				
			$\rho_{s,lean}$	667 kg/m^3				
			d_p	5 × 5 mm				
			Geldart Type	D				
			Fluidizing Gas	Air				
Huang et al. [18]	Studying the mixing and segregation and underlying mechanisms in binary fluidized beds under steady and transient states.	Pseudo 2D, 0.2 m × 0.015 m	**Solids Phases**	Al_2O_3 & quartz sand / Polypropylene plastics and quartz sand	T_{bed}	$T_{Ambient}$	Capacitance probe used to obtain vertical profiles and quantify mixing via an index.	Fast mixing for similar densities, whereas large density differences cause inherent segregation. Different regions of segregation are found, which can be counteracted by increasing the fluidization velocity.
					H/D	2.2		
					$H_{b,0}$	0.44 m		
			$\rho_{s,bulk}$ / $\rho_{s,lean}$	1.32 / 0.31	u_g	0.22 & 0.42 / 0.72 & 1.07 m/s		
			d_p	0.15–0.2 / 0.7–0.8 mm	Solids Fraction	50:50%$_{vol}$		
			Geldart Type	B, D / B, D				
			Fluidizing Gas	Air				

(*continued on next page*)

Table 1 (*continued*)

Reference	Aim of work	Cross-section geometry	Gas and Solids Phases		Operating Conditions		Methodology	Summary
								Mixing in fluidized beds occurs in two stages: macro mixing (rapid, driven by rising bubbles), followed by micro mixing (gradual homogenization). Mixing occurs more efficiently at the bed center than near the walls.
Singh et al. [19]	Assessment of the segregation dynamics of a mixture of Geldart B and D particles	Cylindrical, 0.09 m ID	**Solid Phases**	Glass beads	T_{bed}	$T_{Ambient}$	Electrical Capacitance Tomography (ECT) to quantify segregation regions, rates and times, bubble size distribution and frequency.	Small particles dominate fluidization and bubbling behavior, even at equal mass ratios.
			ρ_s	2550 kg/m^3	H/D	4		
			d_p	0.096 / 0.922 mm	$H_{b,0}$	0.36 m		
			Geldart Type	B / D	u_g	0.02–0.175 m/s		
					Solids Fraction	30–70%$_{wt}$		
			Fluidizing Gas	Air				Higher gas velocity delays segregation by lifting larger particles upward. Flow regimes are chaotic for fine particles and quasi-periodic for coarse particles.
Parvathaneni et al. [20]	Investigation of the effect of local bubbling behavior on the segregation and mixing dynamics of binary mixtures.	Pseudo 2D, 0.2 m × 0.02 m	**Bulk Solids Phase**	Glass beads	T_{bed}	$T_{Ambient}$	Digital imaging and different modes of air injection used to quantify a mixing index and bubble characteristics	Higher lean fraction increases segregation, despite larger and more-frequent bubbles.
			$\rho_{s,bulk}$	2600 kg/m^3	H/D	1		
			d_p	2.26 mm	$H_{b,0}$	0.2 m		
			Φ_s	~1	u_g	1.736 / 2.78 m/s		
					Lean Fraction	30 / 50 / 70%$_{wt}$		
			Lean Solids Phase	SAGO beads				Mixing dominates at high fluidization velocity.
			$\rho_{s,lean}$	1300 kg/m^3				Gas jet distributors reduce segregation by enhancing local circulation compared to uniform distributors.
			d_p	2.32 mm				
			Φ_{lean}	~1				
			Fluidizing Gas	Air				
Windows-Yule et al. [21]	Studying the influence of shape of lean solids on spatial distribution	Cylindrical, 0.07 m ID 0.1 m ID	**Bulk Solids Phase**	Sand	T_{bed}	16 °C	Positron Emission Particle Tracking (PEPT) to obtain vertical distribution profiles summarized by an index.	Density dominates vertical distribution while particle shape has little effect.
					H/D	1 / 2		
					$H_{b,0}$	0.07 / 0.138 m		
			$\rho_{s,bulk}$	2800 kg/m^3	u_g	1.4–2.8 u_{mf}		
			d_p	0.3 mm	Lean Fraction	1%$_{wt}$		
			Φ_s	0.9	Aspect ratio of Lean	0.04 / 0.76 / 1.92 / 5.12		
			Geldart Type	B				
			Lean Solids Phase	Aspherical plastics				
			$\rho_{s,lean}$	1250 kg/m^3				
			d_p	0.4 / 2.8 / 5.2 / 10 mm				
			Geldart Type	D				
			Fluidizing Gas	Air				
Windows-Yule et al. [22]	Investigation of the influence of different distributor designs on fluidization and mixing quality	Cylindrical, 0.07 m ID	**Bulk Solids Phase**	Sand	T_{bed}	16 °C	Positron Emission Particle Tracking (PEPT) to measure dead volume, mixing, and flow patterns.	More orifices improve fluidization and mixing.
					H/D	2		
					$H_{b,0}$	0.14 m		
			$\rho_{s,bulk}$	2800 kg/m^3	u_g	2.4 u_{mf}		
			d_p	0.28–0.34 mm	Lean Fraction	10%$_{wt}$		Orifices near walls reduce dead zones but do not improve mixing.
			Φ_s	0.9				

(*continued on next page*)

Table 1 (*continued*)

Reference	Aim of work	Cross-section geometry	Gas and Solids Phases		Operating Conditions		Methodology	Summary
			Geldart Type	B				
			Lean Solids Phase	Glass beads				Good fluidization does not always mean good mixing.
			$\rho_{s,lean}$	1250 kg/m^3				
			d_p	1 mm				
			Geldart Type	D				
			Fluidizing Gas	Air				
Huang et al. [23]	Assessment of mixing behavior of small binary particles	Pseudo 2D, 0.3 m × 0.02 m	**Solid Phases**	Corundum & silicon carbide / Quartz sand & Walnut shell particles	T_{bed}	$T_{Ambient}$	Capacitance probes and high-speed camera to measure concentration and quantify mixing and entropy.	Fine particles mix slower but more uniformly than coarse particles.
					$H_{b,0}$	0.4 m		
					u_g	1.18–1.48 u_{mf}		
			ρ_s	3970 & 3660 / 2730 & 1120 kg/m^3	Solids Fraction	50:50%$_{vol}$		
			d_p	0.55 mm				Higher gas velocity speeds up mixing.
			Geldart Type	D				Dense bed and wall regions remain non-uniform, while uniform mixing occurs mainly in the middle and upper layers.
			Fluidizing Gas	Air				
Emiola-Sadiq et al. [24]	Investigation of the mixing and segregation of binary mixtures.	Cylindrical, 0.145 m ID	**Bulk Solids Phase**	Silica sand	T_{bed}	$T_{Ambient}$	Frozen bed and digital imaging used to quantify mixing index and vertical and radial profiles of the lean phase.	Mixing happens much faster at the top of the bed than at the bottom
					H/D	1.5		Mixing behavior depends on particle size/shape and loadings.
			$\rho_{s,bulk}$	2650 kg/m^3	$H_{b,0}$	0.22 m		Coarse lean solids fluidize more readily than fine lean solids.
			d_p	0.329 mm	u_g	1–4 u_{mf}		
			Φ_s	~1	Lean Fraction	0–30%$_{wt}$		
			Lean Solids Phase	Biomass (Soyhull pellet / Oathull pellet / Sawdust)				Higher fluidization velocity enhances mixing for cylindrical lean solids.
			$\rho_{s,lean}$	1543 / 1342 / 1511 kg/m^3				
			d_p	10 × 5 mm / 7 × 5.5 mm / 1120 μm				Fine lean solids phase mixes well at low loading levels (<20%$_{wt}$) but mixing declines beyond that.
			Φ_{lean}	0.347 / 0.339 / –				
			Fluidizing Gas	Air				Large and cylindrical lean solids phase shows enhanced mixing with lean fraction.
Roy et al. [25]	Assessment of velocity distribution and local flow patterns of solids	Cylindrical, 0.1 m ID	**Solid Phase**	Glass beads	T_{bed}	$T_{Ambient}$	Radioactive Particle Tracking (RPT) and frozen bed technique to obtain axial and radial velocities and solids diffusivity	Particles circulate in a single large loop, rising at the center and descending along the walls.
					H/D	1.5		
			ρ_s	2500 kg/m^3	$H_{b,0}$	0.36 m		
			d_p	0.5 / 2 mm	u_g	1.1–2.1 u_{mf}		Fine particles move faster than coarse particles.
			Geldart Type	B	Solids Fraction	10 / 30 / 40%$_{wt}$ of coarse particles		
			Fluidizing Gas	Air				Higher loadings of coarse particles increase voidage and impede solids motion.
Li et al. [26]	Studying the mechanism of particle motion of solids under pulsating fluidization conditions.	Cylindrical, 0.1 m ID	**Solid Phases**	Plastic beads / Glass beads	T_{bed}	$T_{Ambient}$	Digital imaging used to quantify a segregation index.	Pulsating reduces drag and enhances density-based segregation.
			ρ_s	1650 / 2400 kg/m^3	H/D	0.8 / 1.2 / 1.6 (3D)		
			d_p	3 mm		1 (2D)		

(*continued on next page*)

Table 1 (*continued*)

Reference	Aim of work	Cross-section geometry	Gas and Solids Phases		Operating Conditions		Methodology	Summary
			Φ_s	~1				As pulsation frequency and gas velocity increase, segregation initially increases, only to decrease subsequently.
		Pseudo 2D, 0.1 m × 0.02 m	Geldart Type	D	$H_{b,0}$	0.080 / 0.12 / 0.16 m (3D) 0.1 m (2D)		
			Fluidizing Gas	Air	u_g	1.1–1.7 u_{mf}		
					Solids Fraction	75:25%$_{vol}$ (3D) 50:50%$_{vol}$ (2D) of plastic beads		
Del Duca et al. [27]	Development of a predictive model for improving the mixing of binary mixtures	Cylindrical, 0.1 m ID	**Bulk Solids Phase**	Fine quartz sand / Coarse silica sand / Fine commercial γ-alumina powder / Ultra-fine commercial γ-alumina powder / Coarse commercial γ-alumina spheres	T_{bed} H/D $H_{b,0}$ Lean Fraction	$T_{Ambient}$ 2.2 ~0.22 ± 0.02 m 25 / 50 / 75%$_{wt}$	Piezo-resistive pressure sensors and visualization used to obtain characteristic velocities.	Density difference prevails over size difference in segregation. At minimum fluidization velocity, the lighter lean phase remains segregated and has little impact on the fluidization of the bulk phase.
			$\rho_{s,bulk}$	2813.5 / 2650.6 / 3986.9 / 3986.9 / 3986.9 kg/m^3				
			d_p	0.1–0.25 / 0.15–0.4 / 0.05–0.25 / 0.063–0.18 / 0.2–0.4 mm				
			Lean Solids Phase	Fine orange peels / Coarse orange peels / Fine tomato peels				At higher gas velocities, the lean fraction exerts influences on fluidization behavior, i.e., slugging, channeling or segregation.
			$\rho_{s,lean}$	671.7 / 671.7 / 1049.9 kg/m^3				
			d_p	1–2 / 5 × 5 / 1–2 mm				
			Fluidizing Gas	Air				Fluidization velocities of binary beds increase with fraction of larger and lighter lean phase.
Werner et al. [28]	Assessment of the mixing dynamics of a mixture of Geldart B and D particles.	Cylindrical, 0.094 m ID	**Solid Phases**	Silica sand / Microcrystalline cellulose	T_{bed} H/D $H_{b,0}$	$T_{Ambient}$ 2 0.188 m	Positron Emission Particle Tracking (PEPT) used to quantify minimum fluidization velocities, micro–macro mixing, flow patterns, and bubble behaviors across different loadings.	Mixing rate and fluidization quality found to be less impacted for up to ≈20%$_{vol}$ loading of lean phase.
			ρ_s	2800 / 1460 kg/m^3	u_g	3 u_{mf}		
			d_p	0.32 / 1.2 mm	Solids Fraction	0–90%$_{vol}$ of microcrystalline cellulose		
			Φ_s	0.917 / 0.94				
			Geldart Type	B / D				Higher fraction of Geldart D solids lean phase lowers the mixing rate.
			Fluidizing Gas	Air				
Molignano et al. [29]	Investigation of mixing and segregation patterns in a hot fluidized bed	Cylindrical, 0.078 m ID	**Bulk Solids Phase**	Silicon Carbide	T_{bed} H/D $H_{b,0}$	500 °C 2 0.148 m	needle-type capacitance probes to obtain space-resolved concentrations summarized by axial dispersion coefficient.	Increasing gas velocity causes layer inversion, dense/fine particles segregate to bed surface while light/coarse particles sink to dense bed.
			$\rho_{s,bulk}$	3253 kg/m^3	u_g	0.34–0.87 m/s		
			d_p	0.505 mm	Lean Fraction	1%$_{wt}$		
			Φ_s	0.63				
			Geldart Type	B				
			Lean Solids Phase	γ-alumina				
			$\rho_{s,lean}$	1209 kg/m^3				
			d_p	1 mm				
			Φ_{lean}	1				
			Geldart Type	D				
			Fluidizing Gas	Air				

global flow characteristics of the bulk solids, including residence times and circulation rates in unary fluidized beds, and more recently assessing velocity distribution [37–42]. However, to date, neither the use of MST for characterization of in-bed dynamics, nor for the study of light particles have been reported. The achievement of robust, high-fidelity signals using only slightly magnetic particles, combined with spatially localized measurements at high temporal resolution, are novel aspects of the present work. Since mixing and segregation are inherently spatiotemporal processes, the concentration profiles resolved in both these dimensions are essential for developing a more-complete understanding.

In addition, regarding studies performed under ambient conditions, the concern remains as to whether the bed dynamics established are representative of those seen at high temperatures. The temperature alters the density and viscosity of the gas and, thereby, the key fluid dynamic variables governing the gas-solids (and potentially also the solid-solid) interactions. The Archimedes and Reynolds numbers under hot conditions (900 °C, for example) are 1–2 orders of magnitude lower than under ambient conditions, yielding different fluidization behaviors [43–45]. The use of fluid dynamic scaling laws is, therefore, recommended to replicate appropriately the behaviors of large-scale, high-temperature operations under ambient conditions. These laws ensure the dynamic, kinematic and geometric similarities between a real unit and a cold model [46,47], guaranteeing that the extracted information has quantitative relevance for the industrial operation. Several studies have experimentally proven the validity of fluid-dynamic scaling laws for gas-solids flows, demonstrating their ability to provide accurate representation of fluidized bed dynamics [48,49], including validation of fuel mixing in sand beds [50]. However, the application of scaling laws implies careful selection of the gas-solids combination without compromising safety or the budget [51]. As a consequence, researchers have often chosen to conduct experiments using the same gas-solids combination as in the hot application, thereby overlooking the discrepancies in the fluid-dynamic behaviors. The findings extracted from such experiments are not automatically extensible to high-temperature industrial operations, and the extent of the quantitative deviation in the data remains unknown.

Chaos analysis offers a complementary perspective to fluid dynamic scaling laws to study dynamics of fluidized beds, providing insights beyond conventional time-averaged or spectral analyses [52,53]. Applying chaos analysis requires selecting appropriate characteristic variables and adjusting operating parameters to maintain dynamic similarity [54]. In binary beds, chaotic motion alone does not guarantee effective mixing and the choice of property used to assess mixing is critical. Global indicators, such as pressure fluctuations or void fraction, primarily reflect bulk bed dynamics and bubble activity and may not capture the behavior of a segregating lean phase, which can evolve differently from the bulk solids. Local measurements of both solids phases are therefore necessary to account for mixing or segregation [55]. When combined with temporal autocorrelation of each solids phase, chaos analysis can reveal particle circulation and the persistence of segregated regions, providing a measure of effective mixing that can be complemented by mixing indices [55]. While chaos analysis with autocorrelation can provide useful insights, its application in density-driven binary beds requires careful interpretation, as the coupled dynamics of buoyancy and drag influence phase-specific mixing.

Computational fluid dynamics (CFD) tools have also been used to investigate mixing and segregation in binary fluidized beds [56–61]. However, challenges persist in relation to dealing with particles with significantly different sizes, as the models require validated correlations for momentum exchange between the two solid phases [62,63] and, within Eulerian frameworks, a multi-grid approach often needs to be adopted [64]. Moreover, the predictive capability of CFD tools is limited by the scarcity of experimental data suitable for rigorous validation; the available measurements are typically restricted to specific locations, such as the dense bed surface, or are derived from pseudo-2D systems. Semi-empirical modeling is also used for examining mixing phenomena in binary beds [65,66], as this methodology offers reliable simulations commensurate with the level of detail that the experimental input provides, although it lacks the generic validity intended in CFD. Thus, developing more-accurate experimental techniques is critical to supporting the predictive capabilities of CFD models for binary fluidized systems [67,68].

In summary, the reviewed literature reveals persistent gaps in the current understanding of solids mixing and segregation in binary fluidized beds. In particular, there exist knowledge gaps in relation to: (i) the lack of measurements made under high-temperature or industrial conditions, limiting the applicability of findings to real-life operational scenarios; (ii) the spatiotemporal resolution of solids concentration, preventing accurate descriptions of how lean solids phase distributions evolve; (iii) the mechanisms underlying mixing and segregation (while general trends are well identified, the underlying physical processes are not well characterized); and (iv) the timescales of mixing and segregation. These knowledge deficiencies hinder the development of predictive models, as well as the optimization of the design and operation of large-scale binary fluidized beds.

The primary aim of this study is to address these knowledge gaps by characterizing the vertical distribution and the dynamics of solid phases in a binary fluidized bed under relevant operational conditions. Towards this goal, the present work develops a measurement technique that applies a novel configuration of magnetic solids tracing to acquire time- and space-resolved concentration profiles of the lean solids phase, thereby enabling quantification of the: (i) mixing indices; (ii) characteristic transition times between the mixed and segregated states; and (iii) dominant frequencies for mixing. This study restricts its scope to binary beds with a coarser and lighter lean phase, so as to be representative of beds of sand and ash (Geldart B solids) that convert some typical solid feedstock (biomass, waste, plastic, peat, coal). The effects of operating conditions, i.e., the fluidization velocity, the bed height, and the loading of the lean solids phase, are investigated under ambient (cold flow) conditions, while preserving the hydrodynamic similarity with large-scale, hot units (using scaling laws).

2. Methodology

2.1. Experimental setup

A reference case is used in the present study, corresponding to the pyrolysis of biomass in a bed of hot sand fluidized by flue gas. The reference unit has a squared cross-section of 1.15 × 1.15 m^2 and is operated at 700 °C. By using full Glicksman's scaling laws [46], such a system is simulated under ambient conditions using a bed with a cross-section of 0.3 × 0.3 m^2 where ambient air fluidizes the bronze powder and a lean phase, which consists of coarser and lighter chip-like synthetic particles (representing biomass). A summary of the relevant parameters used for fluid-dynamic scaling is provided in Table 2. By preserving all relevant dimensionless numbers, the simulated system reproduces the hot-reference hydrodynamics, while secondary parameters, such as particle size distribution, shape, or mechanical/chemical/thermal properties of both solids phases, are not explicitly accounted for as they are not expected to affect the mixing behavior significantly.

Fig. 1 illustrates the experimental setup. The bed is composed of acrylic glass and is equipped with a windbox and a perforated plate for gas distribution. The gas flowrate is regulated by a mass flow controller. Local concentrations of the lean solids phase are measured online at seven vertical positions using magnetic solids tracing (MST; for details on the measurement principle see [37]). For this purpose, seven impedance coils are mounted along a 1 cm outer diameter (o.d.) pin (see close-up of MST pin in Fig. 1). Each coil detects the concentration of magnetic lean solids within a radius of 2 cm from the vertical axis of pin. In the present study, possible inhomogeneities in the lateral direction are not examined, instead representativeness of the data is guaranteed

by long and repeated measurements. Alternatively, multiple MST pins could be used (if placed far apart), this could however become counteractive, provided the intrusive nature of the pin-probe.

The lean phase particles are fabricated from a synthetic expanded foam that is doped with a magnetic powder, so as to make them detectable by the MST coils. Given the wide variability of biomass regarding physical characteristics, a representative set of properties was selected (see Table 2). The design of these particles considers also compatibility with the magnetic solids tracing (MST) technique, ensuring robust and high-fidelity measurements.

The impedance signal, acquired at 100 Hz from each coil, is converted to a concentration of lean phase solids using a calibration curve tailored to each coil (see Appendix A). Two probes immersed in the bed are used to acquire the pressure data used for determining the bed voidage and bubble dynamics. The sampling rate for this measurement is also 100 Hz, and the probes are fixed at vertical positions corresponding to one-half and three-quarters of the static bed height, respectively. The pressure transducers were calibrated and connected to the probes using short, rigid tubing to minimize signal attenuation and phase lag, while the superficial gas velocity was precisely controlled with a mass flow controller. To reduce measurement uncertainty, all results were ensemble-averaged.

Three experimental conditions, namely bed height, loading of the lean solids phase, and fluidization velocity, were systematically varied, as summarized in Table 3. Each experimental case was repeated three times to ensure the representativeness of the acquired data. This aggregation of the data helps to mitigate the impact of horizontal maldistribution of the lean solids phase, which is particularly strong in cases with low loadings of the lean solids phase. In addition, for the experimental conditions in which the lean solids phase was spread over a height interval > 10 cm (the distance between the first and last coils in the pin probe), the experiment was repeated using multiple vertical positions of the MST pin probe. In those cases, three repetitions of the measurements for each position were performed. The resulting data were merged into a single vertical concentration profile.

2.2. Experimental procedure

The experiments were designed to capture the vertical distribution of the lean solids phase both under the steady state (for a given combination of experimental conditions) and during the transitions between the mixed and segregated states induced by sudden changes in the fluidization velocity. Fig. 2a exemplifies the course of an experiment, followed according to the measured local concentrations of the lean solids phase. For the experimental condition shown in Fig. 2, the pin probe was placed at two different vertical positions, yielding a concentration profile over a height > 10 cm and comprising 14 local measurements ($2 \times 7 = 14$ coils). For each run, the unit was first loaded with the amounts of bulk and lean solids phases corresponding to the intended experimental case. The pin and pressure probes were set in place and secured. The binary bed was then fluidized at a fluidization number (FN) of $u_g/u_{mf} = 3$ (based on the u_{mf} of the bulk solids phase) for 60 s, so as to remove possible inhomogeneities in the gas distribution associated with the formation of dead zones and to ensure a good horizontal distribution of the lean solids phase. The fluidization velocity was then set to $u_g/u_{mf} = 1$, and the MST and pressure sampling systems were started. After 60 s of sampling under minimum fluidization conditions (Initial Segregated Steady State in Fig. 2a), the fluidization velocity was increased to the desired test conditions. The bed then transited from the initial segregated state to the mixed state (Transition to Mixing), reaching a steady state with mixing quality being dependent upon the fluidization conditions. After 180 s, the fluidization velocity was reduced back to the minimum fluidization velocity (Final Segregated Steady State), and the bed transitioned from the mixed state to a new steady state (Transition to Segregation). Data acquisition continued for an additional 60 s, after which the experiment was concluded. These five identified distinct steps in the sequence are illustrated in Fig. 2a.

Fig. 2b presents the vertical profiles of the lean phase concentration obtained for the two segregated states (initial and final) and the mixed state. Each datapoint represents a time-averaged value calculated over the corresponding period with steady-state conditions and the bars signify the standard deviations of the corresponding time series.

To assess the consistency of the concentration measurements, a mass balance check was performed (Table 4). For each condition, the loaded mass of lean solids was compared to the mass calculated based on concentration measurements, assuming a perfect distribution of the lean solids over the cross-section of the unit at every height. For this calculation, the profile obtained from the mixed state was used. Overall, the lean phase inventory reconstructed from concentration measurements was in good agreement with the loaded mass, indicating the consistency of the measurements. Larger deviations were observed at the lowest fluidization velocities and lower loadings, where the lean solids visibly showed maldistribution over the bed cross-section and tended to accumulate near the pin. Some discrepancies were also observed for the cases of highest loading and highest velocity, presumably due to larger fluctuations of the signals. While mapping the entire cross-section is not feasible, the measurements were repeated over sufficiently long durations to ensure that the observed trends reliably reflect the distribution of lean solids.

Table 2
Properties of the solid phases and fluidization gas, operational conditions, and scaling parameters for the cold flow model and the resembled hot reactor.

Parameter		Hot reactor simulated	Cold flow model used
Operational conditions	Temperature [°C]	700	20
	Pressure [atm]	1	1
	Minimum fluidization velocity [m/s]	0.16	0.082
		Flue gas	Air
Fluidization gas	Density [kg/m^3]	0.36	1.20
	Viscosity [N/(m•s)]	4.07e-5	1.83e-5
		Sand	Bronze
Bed material bulk solids	Particle density [kg/m^3]	2600	8492
	Mean particle size [mm]	0.789	0.189
		Biomass	Synthetic tracer
Lean solid phase	Particle density [kg/m^3]	500	1,600
	Mean particle size [mm]	20–30	6–8
	Aspect Ratio (L/D)	1.5	1.5
	Density ratio	7,163	7,163
Dimensionless Numbers	Archimedes number	2,742	2,049
	Reynolds number at U_{mf}	1.13	1.02
Scaling factors $\left[\frac{\text{cold}}{\text{hot}}\right]$	Length	0.26	
	Time	0.509	
	Mass	0.06	

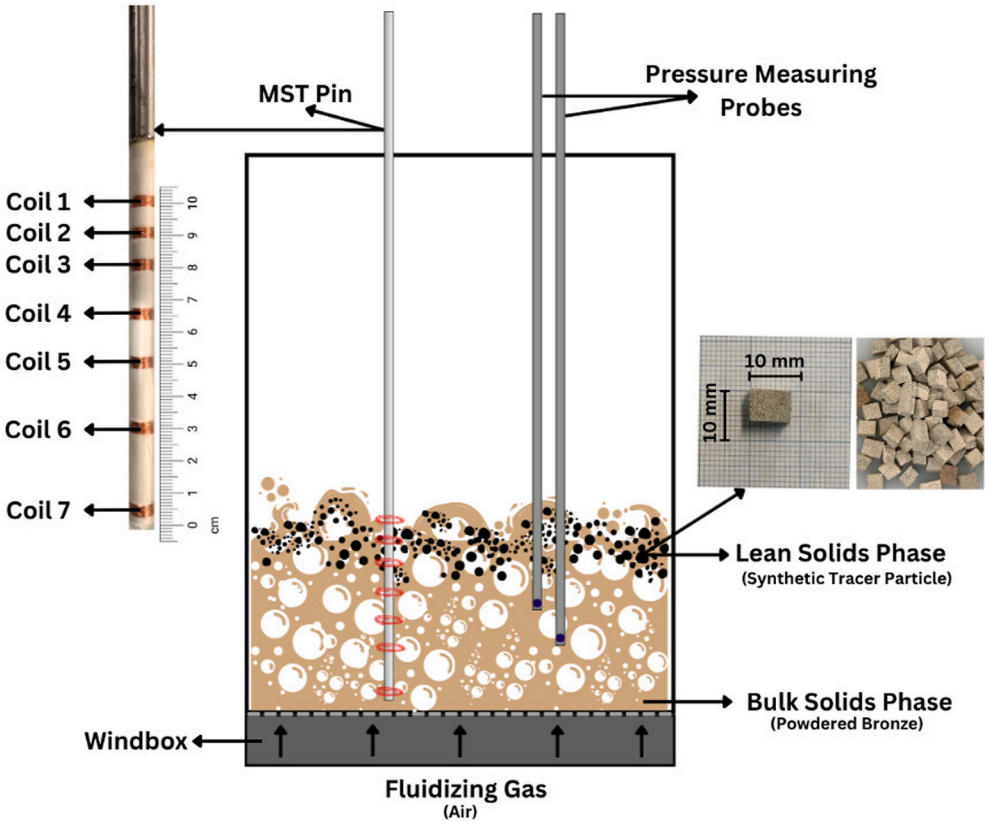

Fig. 1. Schematic of the experimental cold-flow setup (0.3 × 0.3 m^2 in cross-section, resembling an up-scaled bed of 1.15 × 1.15 m^2), representing the magnetic solids tracing (MST) pin and the pressure measurement probes, and presenting details of the MST coils and the magnetic lean solids-phase particles.

Table 3
Test matrix used in the present work. Values in parenthesis indicate the corresponding hot-reference conditions, calculated using the scaling factors listed in Table 2.

Static bed height $H_{b,0}$ [m]	Aspect ratio H/D [−]	Loading of lean solids phase $\varkappa_{lean}$ [$\%_{vol}$]	Mass of lean solids phase m_{lean} [kg]	Fluidization number $\left(\frac{u_g}{u_{mf}}\right)$ FN [−]
0.08 (*0.3*)	0.27	3	~0.36 (*6*)	1.5–4
0.08 (*0.3*)	0.27	5	~0.62 (*10.4*)	
0.04 (*0.15*)	0.13		~0.62 (*10.4*)	
0.08 (*0.3*)	0.27	10	~1.22 (*21*)	
0.12 (*0.46*)	0.4		~1.92 (*32*)	
0.08 (*0.3*)	0.27	20	~2.92 (*48.7*)	

2.3. Data processing and analysis

The volumetric concentrations of each of the three phases present in the binary bed (gas, bulk solids and lean solids) are calculated by solving the following system of equations. In the first place, the sum of the volumetric concentrations must be unity, such that:

$$\varepsilon_g + \varepsilon_{s,bulk} + \varepsilon_{s,lean} = 1 \tag{1}$$

These three volumetric concentrations determine the resulting local bed density according to:

$$\rho_{bed} = \rho_{s,bulk}\varepsilon_{s,bulk} + \rho_{s,lean}\varepsilon_{s,lean} + \rho_g\varepsilon_g \tag{2}$$

Furthermore, the bed density relates to the vertical pressure drop as follows:

$$\Delta P = \rho_{bed} g \Delta h \tag{3}$$

In this work, $\varepsilon_{s,lean}$ is obtained from measurements using the MST pin, while the bed density is calculated through Eq. (3) based on the measured pressure difference between two vertically spaced pressure probes, thus determining the system of equations.

The overall mixing quality is assessed by comparing the mixed and segregated states (refer to Fig. 2b), and quantified using the mixing index (M), which is defined as:

$$M = 1 - \frac{\sigma_{mixed}}{\sigma_{segregated}} \tag{4}$$

This index increases with the extent of vertical mixing, yielding $M = 0$ for complete segregation and $M = 1$ for perfect mixing, and serves as a global indicator and comparison parameter. In the present study, since the focus is on the penetration of the lean solids into the bed of fine solids, the calculation of the mixing index considers only the concentration values acquired inside the dense bed, explicitly excluding datapoints acquired from the splash zone.

Furthermore, the concentration profiles in the mixed state provide the characteristic mixing length, L^*, which is the vertical extent of penetration of the lean solids phase into the dense bed. It is calculated as the distance from the dense bed surface to the lowest position with regular presence of the lean solids phase.

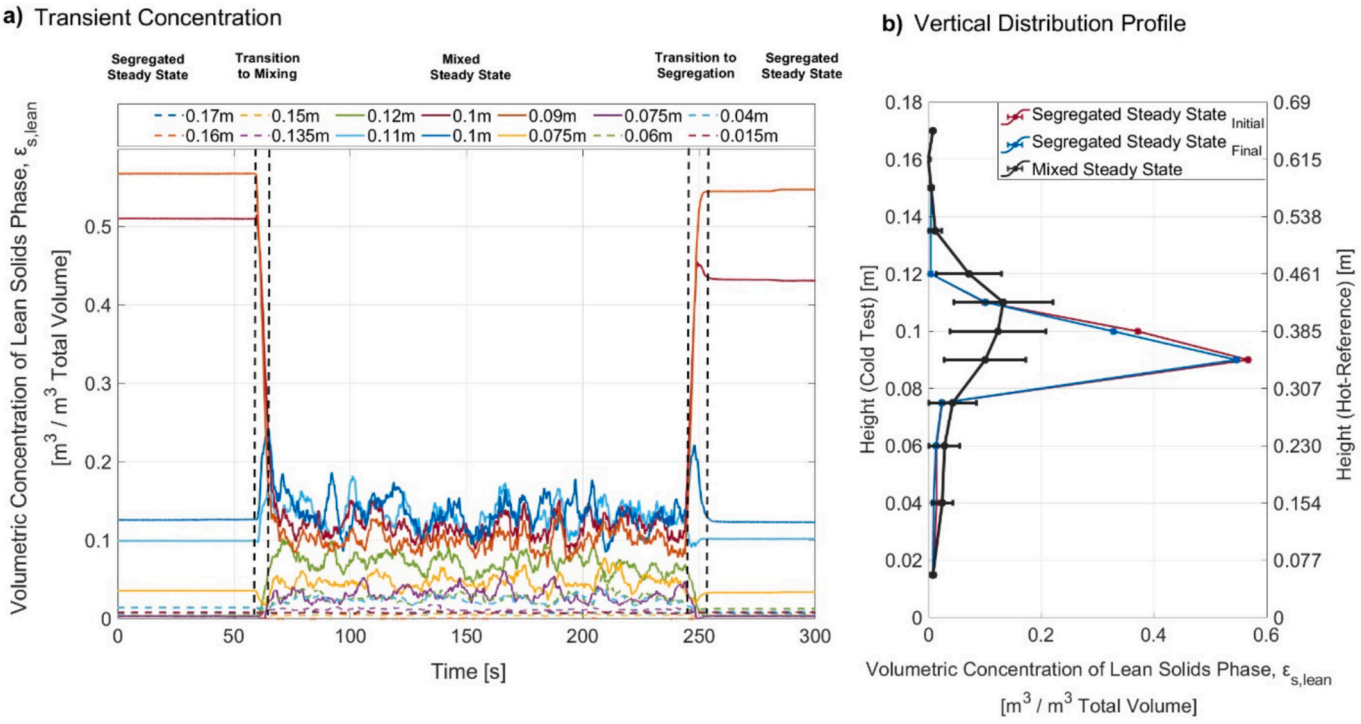

Fig. 2. Example of raw and processed data from one experimental sequence (conditions: $\varkappa_{lean}$ = 10%$_{vol}$, H/D = 0.27, u_g/u_{mf} = 4). a) Measured transient concentrations of the lean solids phase at different heights. The vertical dashed lines indicate the beginning and end of the transition periods (from initial segregated state to mixed state and then to final segregated state, respectively). b) Averaged vertical concentration profiles of the lean solids phases for the mixed (black) and segregated states (red and blue). The horizontal error bars represent the standard deviations of concentration fluctuations at every measured position. (For interpretation of the references to color in this figure legend, the reader is referred to the web version of this article.)

Table 4
Mass balance check. Mass percentages of the lean solids phase calculated based on concentration measurements, as compared to the one calculated based on the loaded mass. Green values indicate a disagreement smaller than 10%, the orange values 10–20%, and the red values indicate a disagreement larger than 20%. The values in brackets indicate the corresponding hot reference conditions, calculated using the scaling factors listed in Table 2.

Bed height ($H_{b,0}$) [m]	Aspect ratio (H/D) [-]	Loading of lean solids phase ($\varkappa_{lean}$) [%$_{Vol}$]	Mass of lean solids phase (m_{lean}) [kg]	Fluidization Number $\left(\frac{u_g}{u_{mf}}\right)$ [-]					
				1.5	2	2.5	3	3.5	4
				Ratio of detected lean solids phase with respect to loaded lean solids mass, [%]					
0.08 (*0.3*)	0.27	3	~0.36 (*6*)	156 ± 2.92	153.7 ± 2.16	147 ± 3.33	150 ± 2.91	154.5 ± 4.33	146.7 ± 2.75
0.08 (*0.3*)	0.27	5	~0.62 (*10.4*)	146.6 ± 2.8	135 ± 2.4	117.2 ± 1.34	108 ± 3.2	108.8 ± 1.91	116.8 ± 2.6
0.04 (*0.15*)	0.13		~0.62 (*10.4*)	107.8 ± 2.3	102.6 ± 3.0	92.8 ± 1.7	93.9 ± 1.3	91.8 ± 2.0	89.7 ± 3.5
0.08 (*0.3*)	0.27	10	~1.22 (*21*)	112.4 ± 3.5	104.3 ± 0.6	90.6 ± 1.1	88.8 ± 1.4	86.6 ± 2.2	85.8 ± 1.2
0.12 (*0.46*)	0.4		~1.92 (*32*)	118.3 ± 5.6	102.7 ± 3.4	97.5 ± 4.1	93.0 ± 4.7	92.6 ± 3.6	91.0 ± 3.3
0.08 (*0.3*)	0.27	20	~2.92 (*48.7*)	95.35 ± 1.0	94.2 ± 0.36	82.5 ± 0.85	74 ± 0.24	71.4 ± 1.05	71.4 ± 1.45

To assess the mixing behavior of the lean solids phase in relation to the bed dynamics, a power spectral density (PSD) analysis was used. The PSDs were computed using the Welch method. Signals sampled at 100 Hz were filtered using a second-order low-pass filter with a cutoff frequency of 45 Hz, just below the Nyquist frequency of 50 Hz, to suppress high-frequency noise and prevent aliasing. Zero-phase filtering in MATLAB preserved the temporal characteristics of the signal. Signals were divided into segments length of 1024 samples (≈0.1 Hz frequency resolution) with a Hann window applied to reduce spectral leakage. At least 16 sub-spectra per repetition were averaged, resulting in a total of 48 spectra for robust statistical convergence. This analysis determines the dominant frequency and frequency spread of both the pressure fluctuations (associated with the main dynamics of the bed, i.e., bubble flow and bulk solids phase) and fluctuations of the lean solids concentration (associated with its mixing).

The transitions from segregated to mixed state (Mixing Transition) and vice versa (Segregating Transition) are characterized by means of transition times, τ* (see Fig. 2a). To facilitate identification of the

beginning and end of each of these transition periods, the original time series of the impedance signals (sampled at 100 Hz) is filtered using a moving average routine with a window of 500 sample points (i.e., 5 s). The transitional mixing time (τ_{mix}*) is counted from the moment when the fluidization velocity is increased until the time that the first concentration peak appears in the lowest coil with regular presence of the lean solids phase; this is the same coil as that indicating the characteristic mixing length, L*. Analogously, the transitional segregation time (τ_{seg}*) corresponds to the time that elapses from the instant when the fluidization velocity is reset to the minimum to when the signal at the topmost coil (positioned at the bed surface) stabilizes. The characteristic lengths and times introduced above are used to calculate the velocities ($u = L^*/\tau^*$) of the mixing and segregation processes.

3. Results and discussion

Section 3.1 outlines the results for bed voidage, with the information being used for the subsequent analyses. Section 3.2 provides a detailed analysis of the impacts of the operational conditions on the vertical distribution of the lean solids phase, while separate subsections are dedicated to the impacts of fluidization velocity (Section 3.2.1), lean solids phase loading (Section 3.2.2), and bed height (Section 3.2.3). Section 3.3 summarizes the analysis of the mixing index, which is a global indicator of mixing that is used to compare the results across different operating conditions. Section 3.4 explores the dynamic behavior of the binary bed, covering a frequency analysis of both the lean phase mixing and the bed dynamics (Section 3.4.1), as well as the velocities for the mixing and segregating transitions (Section 3.4.2).

3.1. Bed Voidage

Fig. 3 shows the dependency of the time-averaged bed voidage (calculated as described in Section 2.3) on the fluidization velocity, together with the impacts of lean solids phase loading (Fig. 3a) and bed height (Fig. 3b). In Fig. 3b, data for the lowest bed height ($H_{b,0} = 0.04$ m, $H/D = 0.13$) are excluded because the vertical resolution of the MST pin was not sufficient for reliable determination of $\varepsilon_{s,lean}$ and, thus, of ε_g (see Section 2.3). Additional data for unary beds (i.e., beds containing only bulk solids) are provided in Appendix B.

The trend of increasing bed voidage with fluidization velocity, previously reported for bulk solids beds [69–71] and represented by the black line in Fig. 3a, is also evident in the binary beds studied here, regardless of the loading of the lean solids phase and the bed height. As shown in Fig. 3a, bed voidage increases also with loading of the lean solids phase. This can be attributed to two mechanisms: (i) the lighter and larger lean solids disrupt the packing structure in the dense emulsion and, consequently, increase the gas holdup, an effect previously documented in the literature [72]; and/or (ii) the thick segregated layer of the lean solids phase (Geldart D) hinders bubble flow and eruption, increasing bubble residence time in the bed. Regarding the impact of bed height (Fig. 3b), the introduction of a lean solids phase results in the bed voidage increasing with bed height, in contrast to unary beds (for which no significant dependence on bed height is observed; see Appendix B). This increase is attributable to the distortion of the bulk solids packing structure; greater bed height enhances vertical mixing of the lean solids (as will be presented in Section 3.2.3), intensifying the aforementioned mechanisms.

3.2. Vertical distribution of the lean solids phase

3.2.1. Effect of fluidization velocity

Fig. 4 shows the vertical distributions of the lean solids phase for a bed of medium height ($H/D = 0.27$) with 10%$_{vol}$ loading. Horizontal bars indicate the standard deviations, as calculated based on multiple repetitions. Solid lines represent the positions below the dense bed surface, while dashed lines are used for the data collected in the splash zone. All the cases have the same loading of lean solids phase, although the integral of the profiles sometimes diverges from unity (as reported in Table 4) due to inherent lateral maldistribution. In all cases, a distinct concentration peak aligns with the expansion of the dense bed, serving as a reliable indicator of the dense bed height.

At low fluidization velocities, the larger and lighter lean solids phase accumulates near the bed surface. As the fluidization velocity increases, the lean solids phase penetrates deeper into the dense bed and rises further into the splash zone, thereby broadening the vertical distribution and tending towards a more uniform profile. This is attributed to the development of more and larger bubbles that create stronger vertical flows of bulk solids in both of the vertical directions [66,73–75], which in turn drags more of the lean phase solids along the bed height, thereby promoting vertical mixing [76,77].

The fluctuations of the lean solids phase concentration provide further insights into the mixing behavior. For the concentration profiles shown in Fig. 5, the bars represent the mean amplitudes of the fluctuations in concentration at each measurement height. As seen, for the two cases, the data are characterized by significant fluctuations, ranging from values close to 0 (attributable to either bubble passages or simply the absence of lean solids in the emulsion surrounding the coil) to values that are several times the average concentration. This reflects the dynamic character of the lean solids distribution, with particle clusters being constantly transported between different regions along the bed height. However, at low fluidization velocities, the lower bed locations exhibit minimal fluctuations of concentration, indicating low rates of local mixing of the lean solids phase, as previously shown in Fig. 4.

3.2.2. Effect of lean solids loading

To enable comparisons across different loadings, the vertical concentration profiles of the lean solids phase were converted into probability density functions (PDFs) (the corresponding absolute concentration profiles are provided in Appendix C). Fig. 6 compares the different loadings for two selected fluidization velocities. Note that, to facilitate the comparison, the horizontal coordinate uses the position of the dense bed surface as the origin, instead of the bottom plate. At the lower fluidization velocity ($u_g/u_{mf} = 2$; Fig. 6a), the vertical distribution remains essentially unaltered across all loadings, with the lean solids phase largely segregated at the bed surface and showing very limited penetration into the dense bed. As described above, a higher fluidization velocity ($u_g/u_{mf} = 4$; Fig. 6b) yields wider vertical distributions. However, an increase in the loading beyond 5%$_{vol}$ is seen to promote segregation even under these conditions.

The second (ii) mechanism indicated earlier in Section 3.1 becomes apparent at higher loadings. The thick surface layer of the lean solids appears at the bed surface and hinders bubble eruptions, such that they instead split and percolate through the thick layer of lean solids. Consequently, the movement of solids downwards is reduced, which together results in reduced vertical circulation [28]. This effect persists even with increasing fluidization velocity, as only a fraction of the lean solids penetrates the dense bed, whilst a large share remains at the surface.

3.2.3. Effect of bed height

To analyze the effect of bed height, two approaches were used: (i) varying the bed height while keeping the lean phase mass constant (Fig. 7); and (ii) varying the bed height while keeping the lean phase loading (volumetric fraction) constant (Fig. 8).

Fig. 7 shows the vertical distribution of the lean solids phase at two fluidization velocities (absolute concentration profiles are reported in Appendix C). At the lower velocity ($u_g/u_{mf} = 2$, Fig. 7a), the distribution of the lean phase is very similar for the two bed heights, with strong segregation to the bed surface. However, at the higher velocity ($u_g/u_{mf} = 4$, Fig. 7b), there is a clear enhancement of the vertical mixing with an increase of the bed height. Comparing the two plots in the figure, it is seen that the shallow bed is unable to counteract the formation of a

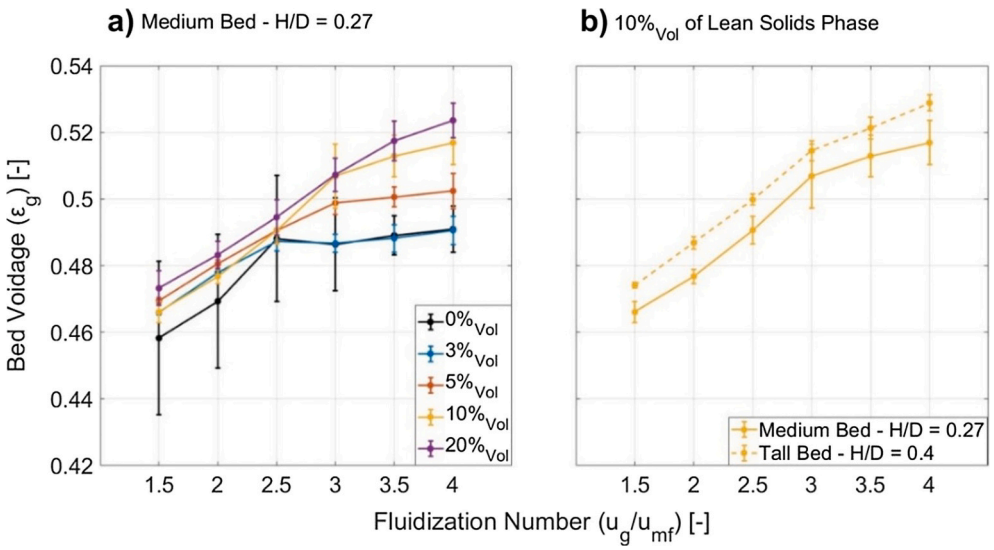

Fig. 3. Time-averaged bed voidage (estimated based on pressure difference measurements) as a function of the fluidization number for: a) varying lean solids phase loading at constant bed height (H/D = 0.27); and b) varying bed height at constant lean solids loadings ($\varkappa_{lean}$ = 10%$_{vol}$).

segregated layer regardless of the increase in velocity, suggesting that, within the velocity ranges investigated, the mixing might be restricted by the limited bubble growth and/or the rising of jets directly from the distributor plate to the bed surface. This interpretation is supported by the significantly higher voidage measured in the shallow unary bed, as compared with the medium and tall beds (see Appendix B).

Fig. 8 shows the vertical distributions of the lean solids for three bed heights at a loading of 10%$_{vol}$ and for two selected fluidization velocities. At the lower fluidization velocity (u_g/u_{mf} = 2, Fig. 8a), the distributions are similar, with narrow peaks indicating accumulation of the lean solids phase near the bed surface, which indicates limited mixing. In contrast, at the higher fluidization velocity (u_g/u_{mf} = 4, Fig. 8b), the vertical distribution of the lean solids phase is spread more broadly for the medium and tall beds. In comparison to Fig. 7, taller beds in Fig. 8 imply also a larger net amount of lean solids phase. Despite this, beds with H/D > 0.27 exhibit a wider vertical distribution of the lean phase, thus showing stronger bed dynamics and more pronounced bubble growth that overcomes the formation of a thick lean solids layer.

3.3. Mixing index

Fig. 9 presents the values of the mixing index [Eq. (4)] for the different experiments. Across all cases, the mixing index increases with fluidization velocity, confirming improved vertical mixing of the lean solids phase. This trend, previously reported in the literature [7,78–82], is associated with intensified bubble activity, as higher fluidization

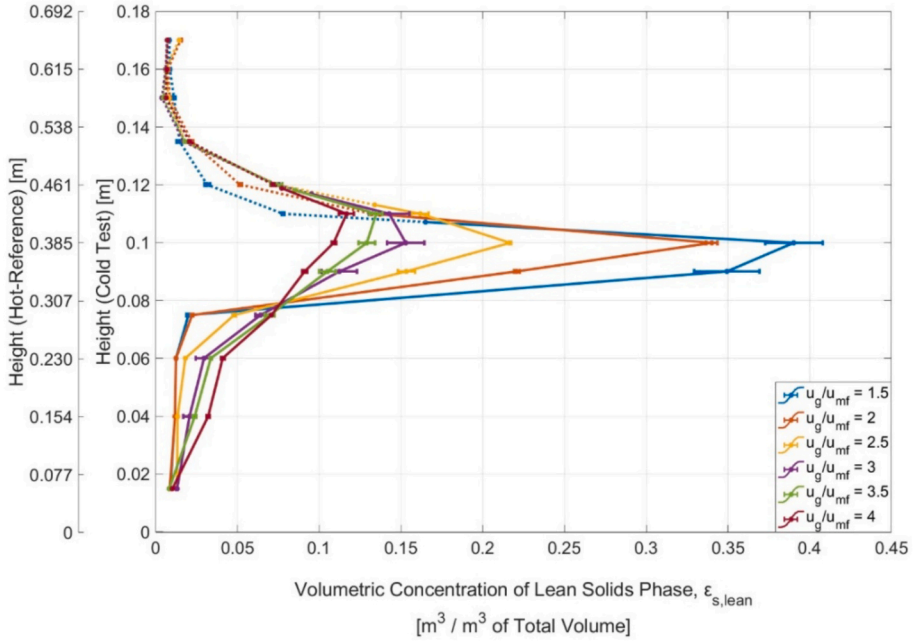

Fig. 4. Time-averaged vertical concentration profiles of the lean solids phase for different fluidization numbers. Conditions: H/D = 0.27, $\varkappa_{lean}$ = 10%$_{vol}$. The solid and dotted lines connect the data obtained for the dense bed and splash zone, respectively, as identified from the bed voidage profile (Fig. 3). The horizontal error bars indicate the standard deviations calculated based on repetitions.

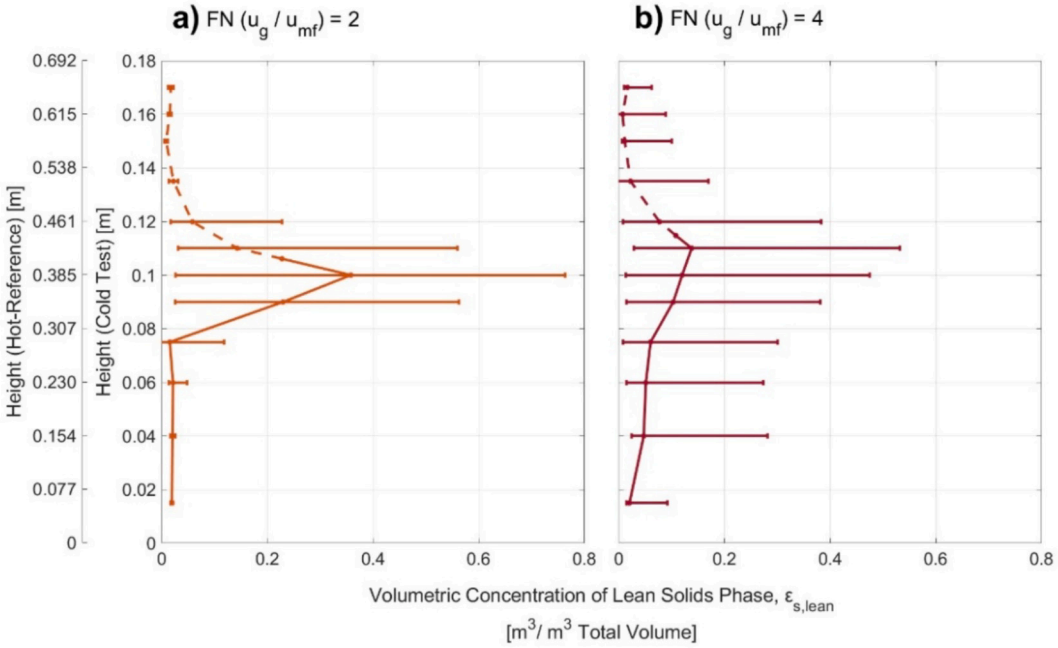

Fig. 5. Time-averaged vertical concentration profiles of the lean solids phase, with horizontal bars indicating the amplitudes of the concentration fluctuations. The solid and dotted lines connect the data for the dense bed and splash zone, respectively, as identified from the bed voidage profile (Fig. 3). Conditions: H/D = 0.27, $\varkappa_{lean}$ = 10%$_{vol}$. a) u_g/u_{mf} = 2 and b) u_g/u_{mf} = 4.

velocities increase the size and rising velocity of the bubbles [3].

Fig. 9a showcases the influence of the loading of the lean solids phase on the mixing. At a given fluidization velocity, the mixing index remains relatively unchanged for loadings up to 10%$_{vol,}$ but it drops noticeably with 20%$_{vol}$ loading. This decrease in mixing index correlates with the observed formation of a thick layer of lean solids phase that accumulates at the bed. The effect of the layer persists regardless of the increase in fluidization velocity (see Fig. 6b), resulting in consistently lower mixing indices. Werner et al. [28] reported a similar behavior for loadings >20%$_{vol}$, although their experiments were conducted without fluid-dynamic scaling, which likely contributed to the different value for the critical loading. Furthermore, for loadings up to 10%$_{vol}$, i.e., below the critical loading, the mixing index seems to reach a saturation value (between 0.7 and 0.8) once the fluidization velocities exceed $u_g/u_{mf} \sim 3$. The above specific values apply to the specific pair of solids used in this study, while qualitative trends should still hold for beds of Geldart B bulk solids with Geldart D lean solids. In contrast, beds composed of another type of bulk solids, e.g. Geldart A, may exhibit different qualitative behavior, whereby substantial loadings of lean solids may act as jetsam and stratify towards the dense bed instead, potentially leading to bed instabilities, including cracking, channeling, or even defluidization [17,56].

Fig. 9b illustrates the influence of bed height on the mixing index at constant mass loading of the lean solids phase. The shallow bed exhibits a low and only slightly increasing mixing index with the fluidization number, whereas the medium bed shows not only considerably higher indexes, but also a marked increase in the index with increased fluidization velocity.

Fig. 9c presents the corresponding results for a constant volumetric loading of 10%$_{vol}$. With increasing bed height, the amount of lean solids

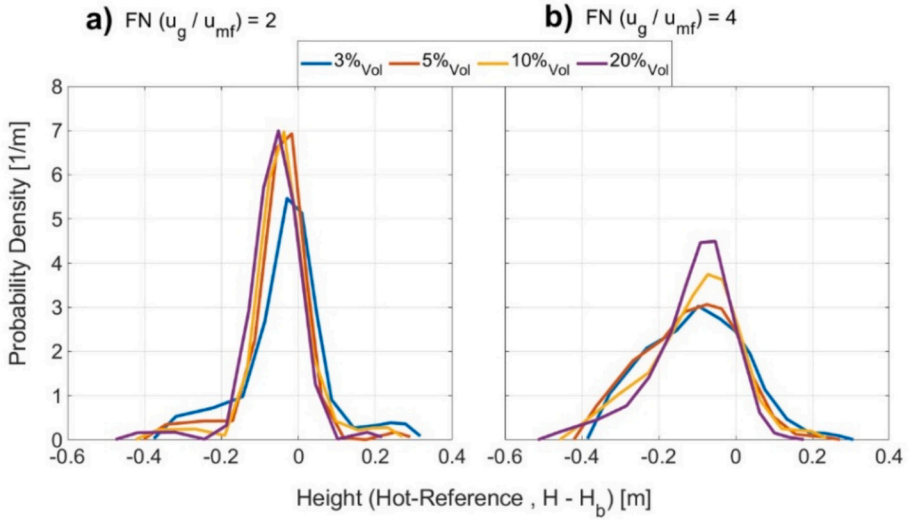

Fig. 6. Probability density distributions of the lean solids phase concentration over the height at different loadings, obtained from time series under steady-state conditions. Conditions: H/D = 0.27. a) u_g/u_{mf} = 2; and b) u_g/u_{mf} = 4.

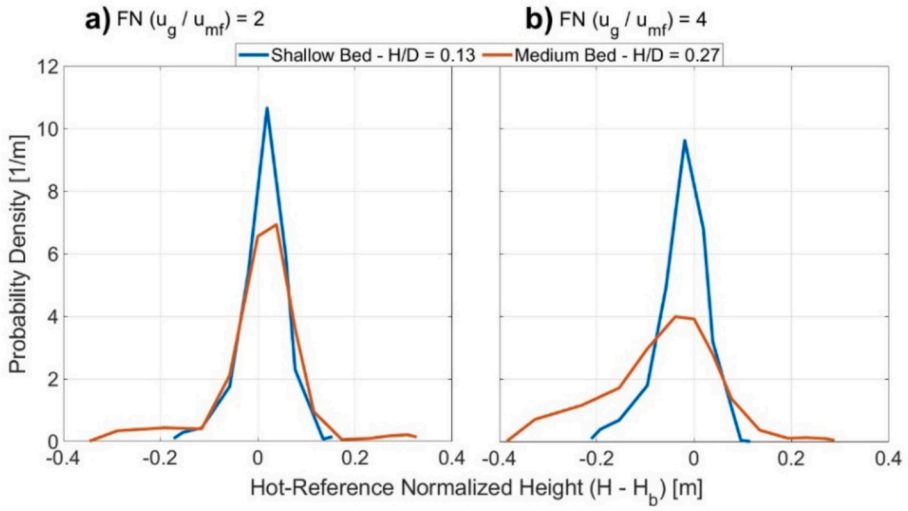

Fig. 7. Probability density functions of the lean concentration over the height for different bed heights at constant mass loading, obtained from steady-state time series. Conditions: $m_{lean} = 10.4$ kg. a) $u_g/u_{mf} = 2$; and b) $u_g/u_{mf} = 4$.

phase becomes larger. However, the mixing index remains almost unchanged between the medium and tall beds, indicating that within the investigated range, mixing is preserved for beds with H/D > 0.27.

3.4. Dynamics

3.4.1. Frequency analysis

Fig. 10 presents the frequency analysis of the cases studied, illustrated through the cumulative frequency spectra of the fluctuations of both the lean phase concentration and the pressure (reported here for hot reference conditions). Fig. 10a shows the data for different fluidization velocities. The pressure fluctuation spectra reveal median frequencies (f_{50}) below 3 Hz that slightly increase with fluidization velocity, which indicates more-frequent bubble formation and gas–solids interactions as the gas velocity increases. These observations are in accordance with the literature [83,84]. The spectra for lean solids concentration follow a similar trend but display consistently lower median frequencies (<1 Hz), suggesting that only about one-third of the bubble events effectively contribute to solids mixing.

Fig. 10b illustrates the frequency spectra for varying loadings of the lean solids phase. Overall, the data indicates that, within the conditions studied, the loading does not significantly impact the lean phase mixing or the bed dynamics. The results for the lowest lean phase loading ($3\%_{vol}$) are not considered here, due to the significant concentration inhomogeneities in the horizontal direction observed under these conditions. Thus, although the time-averaged information is representative, the fluctuations of the concentration are affected by lateral variations.

Fig. 10c displays the spectral distributions for cases with different bed heights. As expected, the pressure spectra indicate higher median bubble frequencies in the shallow bed. However, this increase does not manifest itself in the spectra of the lean solids phase concentration, which shows limited sensitivity to bed height within the range investigated. This means that, despite faster bed dynamics and the presence of more-frequent bubbles, their ability to promote mixing of the lean solids phase is limited, likely due to geometric constraints, smaller bubble size, and high-velocity gas jets. Overall, these results suggest that higher bubble frequency alone is not sufficient to improve mixing quality.

Although the MST pin-probe is invasive and may introduce minor local disturbances, the measured solids fluctuations reflect the inherent bed dynamics. For the operating conditions tested here, including

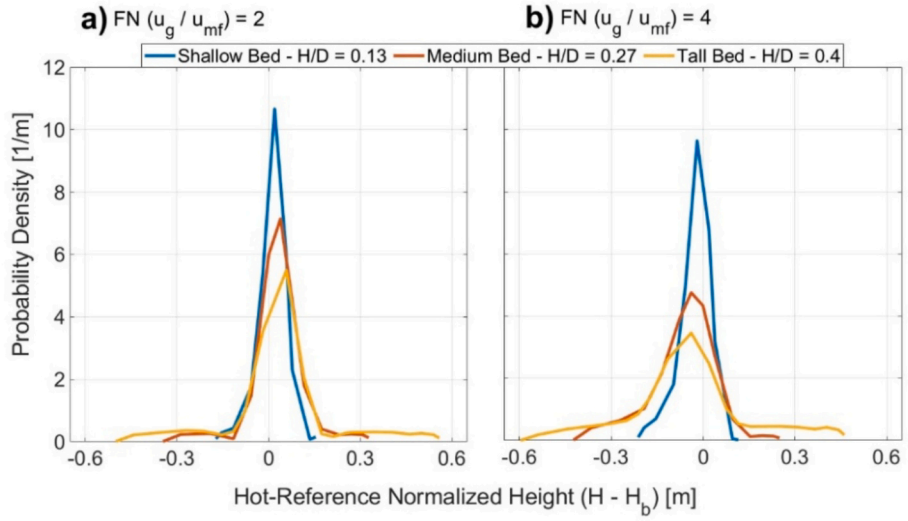

Fig. 8. Probability density functions of the lean solids concentration over the height for different bed heights at constant volumetric loading, obtained from steady-state time series. Conditions: $\varkappa_{lean} = 10\%_{Vol}$. a) $u_g/u_{mf} = 2$; and b) $u_g/u_{mf} = 4$.

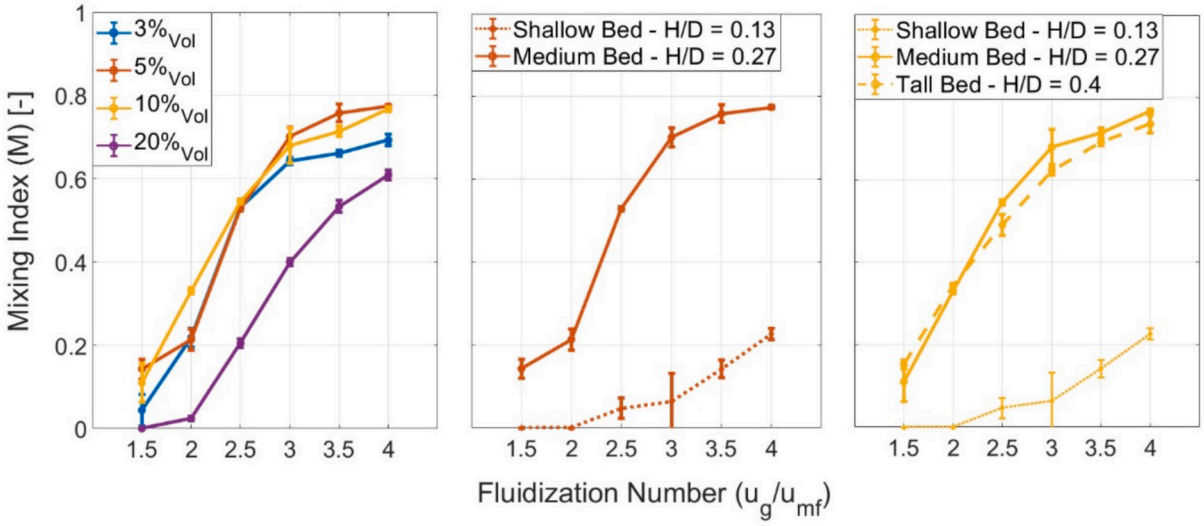

Fig. 9. Mixing index dependency on the fluidization velocity. (a) Varying lean solids phase loading at constant bed height (H/D = 0.27), (b) Varying bed heights at a constant mass (m_{lean} = 10.4 kg), and (c) Varying bed height at constant volumetric loading ($\varkappa_{lean}$ = 10%$_{vol}$).

fluidization velocity, lean solids loadings, and bed height, the effective bubble fraction remains largely unaffected. However, outside these conditions, or for markedly different solid types or systems, the contribution of bubbles to solids mixing may change. Particularly, as shown by previous studies, the distributor pressure drop affects the bubble dynamics [85] altering axial and lateral mixing of lean solids [16,50], which in turn may possibly influence the efficiency of bubble-induced mixing.

3.4.2. *Transitions between mixing and segregation*

The values of the penetration length, mixing time, and segregation time, estimated according to the methodology described in Section 2.3, are listed in Table 5. Consistent with previous results (Section 3.2), the penetration length of the lean solids phase into the dense bed increases with fluidization velocity and bed height, an effect that is associated with larger, faster and more-frequent bubbles and, consequently, well-developed solids flow structures. However, for shallow beds, the penetration length remains largely unaffected by changes in the fluidization velocity. Higher fluidization velocities and taller beds accelerate lean solids mixing and reduce segregation times. Notably, the characteristic segregation times (τ_{seg}^*) are consistently longer than the characteristic mixing times (τ_{mix}^*).

Figs. 11 and 12 present the transitional mixing and segregation velocities, respectively, for all the cases studied. In general, higher fluidization velocities (FN during the mixed stage) lead to higher transitional velocities for both mixing and segregation. Higher fluidization velocities are associated with faster bubble rise and larger wake regions, which in turn promote the movement of solids in the vertical direction. Similarly, when the fluidization velocity is reduced to the minimum from a strongly mixed state with high bed voidage, the system transitions more readily to segregation, as the residual bubbles and voids enhance particle mobility, allowing the lighter and larger lean solids phase to stratify

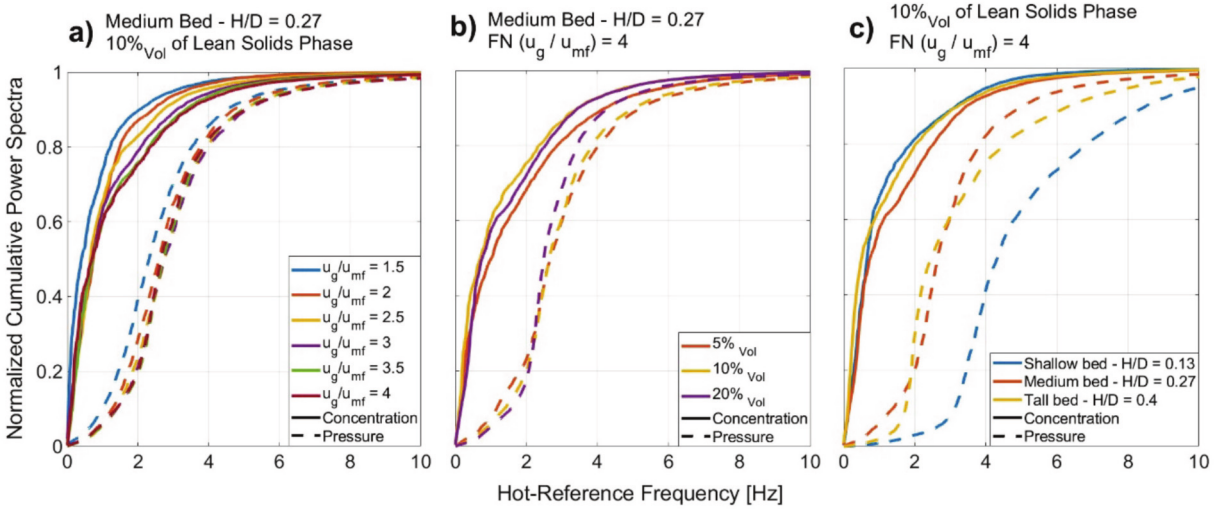

Fig. 10. Cumulative power spectra of the pressure (dashed line) and lean solids phase concentration (solid line) for: (a) varying fluidization velocity at constant bed height (H/D = 0.27) and volumetric loading ($\varkappa_{lean}$ = 10%$_{vol}$); (b) varying lean phase loadings at constant bed height (H/D = 0.27) and u_g/u_{mf} = 4; and (c) varying bed height at constant volumetric loading ($\varkappa_{lean}$ = 10%$_{vol}$) and u_g/u_{mf} = 4.

Table 5
Characteristic scales for mixing and segregation (derived as indicated in section 2.3) for the setup and operating conditions tested in this study (reported values are upscaled for hot-reference conditions using the scaling factors listed in Table 2).

Bed height ($H_{b,0}$) [m]	Aspect ratio (H/D) [−]	Conc. of lean solids phase (x_{lean}) [$\%_{Vol}$]	Mass of lean solids phase (m_{lean}) [kg]	Characteristic Scales (Length and Time)	Fluidization Number $\left(\frac{u_g}{u_{mf}}\right)$ [−]					
					1.5	2	2.5	3	3.5	4
				L* [m]	0.058	0.115	0.115	0.192	0.192	0.288
0.3	0.27	3	~6	τ_{mix}* [s]	12.98 ± 1.6	11.91 ± 2.6	10.47 ± 1.18	13.71 ± 1.7	13.64 ± 0.69	16.67 ± 0.58
				τ_{seg}* [s]	16.19 ± 3.5	18.40 ± 1.07	18.41 ± 0.99	24.86 ± 3.91	24.70 ± 1.8	26.40 ± 4.3
				L* [m]	0.058	0.115	0.115	0.192	0.192	0.288
0.3	0.27	5	~10.4	τ_{mix}* [s]	13.92 ± 2.53	11.88 ± 1.54	11.03 ± 0.67	18.07 ± 4.78	13.08 ± 0.46	16.53 ± 1.42
				τ_{seg}* [s]	13.48 ± 2.96	17.08 ± 1.52	14.36 ± 1.32	21.78 ± 0.44	16.97 ± 1.16	20.02 ± 0.88
				L* [m]	0.038	0.077	0.077	0.077	0.077	0.077
0.15	0.13	10	~10.4	τ_{mix}* [s]	14.04 ± 1.92	18.50 ± 2.04	17.23 ± 1.83	16.7 ± 4.31	15.8 ± 1.83	14.85 ± 0.43
				τ_{seg}* [s]	26.38 ± 9.05	43.71 ± 23.65	26.79 ± 9.16	29.23 ± 2.63	23.63 ± 5.53	13.45 ± 0.81
				L* [m]	0.058	0.115	0.192	0.192	0.192	0.288
0.3	0.27	10	~21	τ_{mix}* [s]	14.49 ± 2.59	10.84 ± 0.61	18.26 ± 3.77	13.92 ± 3.29	13.31 ± 2.03	18.13 ± 4.45
				τ_{seg}* [s]	14.43 ± 0.08	13.70 ± 0.66	16.84 ± 1.37	15.32 ± 1.58	14.49 ± 0.68	17.99 ± 0.65
				L* [m]	0.115	0.115	0.192	0.25	0.31	0.385
0.46	0.4	10	~32	τ_{mix}* [s]	14 ± 0.44	11.11 ± 1.37	15.32 ± 2.76	13.71 ± 2.04	11.91 ± 1.93	13.89 ± 2.10
				τ_{seg}* [s]	18.95 ± 3.93	18.49 ± 2.17	19.98 ± 0.69	22.78 ± 0.72	25.91 ± 0.12	27.18 ± 3.42
				L* [m]	0.058	0.058	0.115	0.115	0.192	0.192
0.3	0.27	20	~48.7	τ_{mix}* [s]	16.65 ± 5.62	11.47 ± 1.01	12.98 ± 0.28	13.17 ± 2.77	14.88 ± 1.97	13.95 ± 1.70
				τ_{seg}* [s]	18.14 ± 1.11	16.53 ± 1.08	19.94 ± 2.0	15.36 ± 0.28	18.83 ± 0.7	17.25 ± 0.55

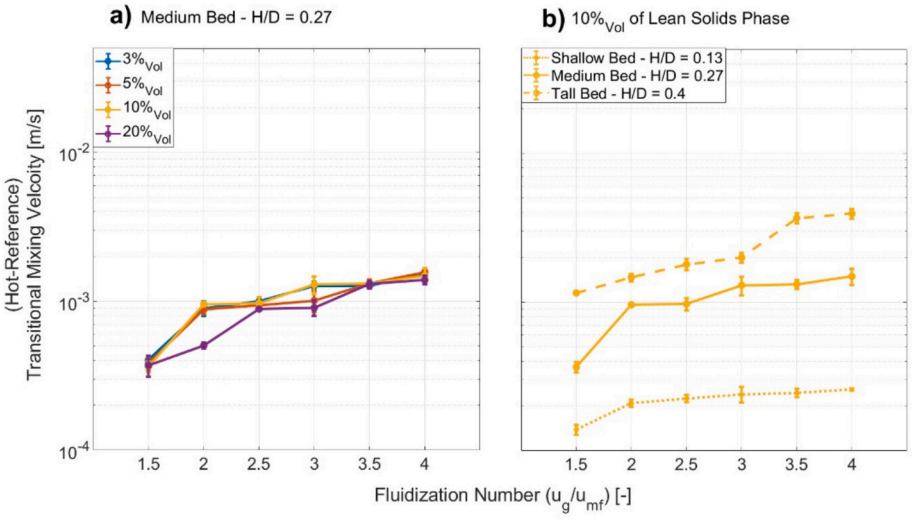

Fig. 11. Transitional mixing velocities in relation to fluidization velocity, determined from characteristic length and times listed in Table 5. (a) Varying lean solids phase loading at constant bed height (H/D = 0.27). (b) Varying bed height at constant volumetric loading (x_{lean} = 10%$_{vol}$).

and accumulate near the bed surface.

Fig. 11a shows that the transitional mixing velocity remains largely unchanged with increasing lean phase loading, with only a slight decrease noted beyond a threshold (x_{lean} = 20%$_{vol}$) at lower fluidization velocities, at which point the thick surface layer of lean solids is able to withstand the bubble mixing impulsion and restricts almost completely the particle mobility. Fig. 11b shows that the transitional mixing velocity increases with bed height. Taller beds provide enhanced mixing and enable the system to reach the mixed steady state more rapidly when the fluidization velocity is increased abruptly.

Fig. 12a shows that the transitional segregation velocity increases with loading and, in similarity to the mixing velocity, tends to drop for the highest loading (i.e., x_{lean} = 20%$_{vol}$) under lower fluidization velocities. This trend is attributable to the slow formation of the layer of lean solids that prevents residual bubbles from reaching the surface and, thereby, limits the mobility of the lean particles despite their lower density and larger size. Fig. 12b indicates that transitional segregation velocities increase with bed height, as more and larger bubbles and stronger flow structures are in place, which facilitate faster particle redistribution during the transition to minimum fluidization. In contrast, in shallow beds, fewer and underdeveloped bubbles may escape the bed almost instantly upon reduction of the fluidization velocity to the minimum, leading to rapid bed compaction and leaving segregation to be primarily governed by the size and density of the lean solids phase.

For transitional mixing and segregating velocities, the trends

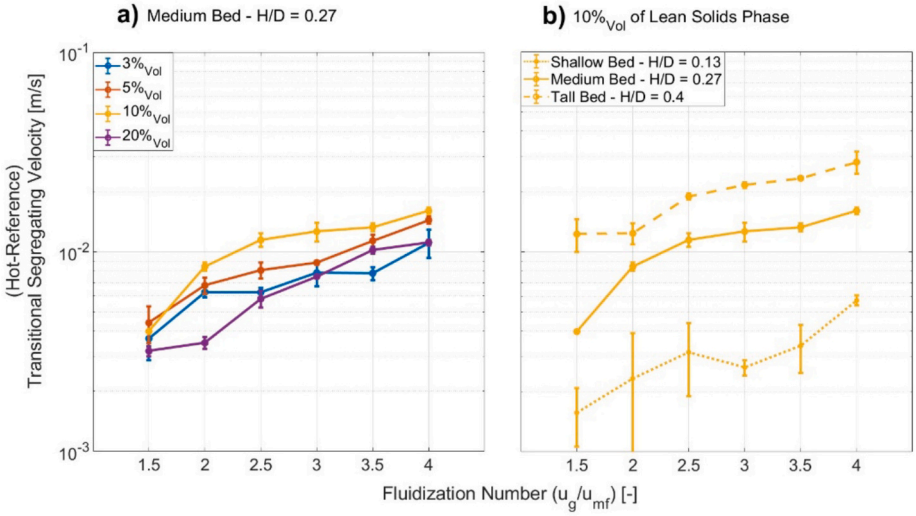

Fig. 12. Transitional segregating velocities, determined from characteristic length and times listed in Table 5. (a) Varying lean phase loading at constant bed height (H/D = 0.27). (b) Varying bed height at constant volumetric loading ($x_{lean} = 10\%_{vol}$).

associated with bed height are similar for both constant mass and constant volumetric loadings, unlike steady-state mixing, where the thickness of the lean solids layer plays a significant role.

4. Conclusion

In the present study, the mixing of a lighter and larger solids phase in a bubbling fluidized bed is investigated in a cold flow model under conditions that resemble large-scale hot operation. A novel pin probe implementation of the magnetic solids tracing technique is used to extract spatiotemporal measurements of the lean solids concentration, deriving descriptions that are more detailed than those available in the literature.

The effects of fluidization velocity, lean phase loading, and bed height on mixing follow trends that are qualitatively consistent with those reported previously in the literature. Discrepancies are attributed to the implementation of fluid-dynamic scaling in the present work. An increase in the fluidization velocity enhances mixing, whereas lean phase loadings beyond a critical threshold value of ~$10\%_{vol}$ leads to the formation of a lean solids layer at the bed surface that dampens the bubble eruptions and reduces the mobility of the lean and bulk solids phases. Bed height and lean solids phase loadings are critical parameters that interact, with the former promoting bubble development and vigorous splashing, and the latter showing a tendency to form a layer of lean solids that hinders bubble eruption and solids vertical mobility. For a given lean solids loading, the fluidization velocity and bed height need to be adjusted to ensure adequate mixing and reduced surface layering of the lean solids phase, as the solids mixing index depends heavily on these parameters. This provides a practical framework for optimizing the performance of a fluidized bed, enabling either effective mixing or controlled segregation through coordinated adjustment of the bed height, lean phase loading and fluidization velocity.

Frequency analyses of pressure and concentration fluctuations reveal distinct time scales. Pressure spectra, dominated by the bubble dynamics (f_{50} ~ 3 Hz), are significantly faster than those for the lean phase concentration (f_{50} ~ 1 Hz), indicating that only a fraction of bubble events (roughly one-third) effectively contributes to solids mixing. While variations in fluidization velocity have limited effects, the bed height influences bubble activity, where shallower beds exhibit bubbles that are more frequent but less effective in terms of contributing to the mixing, probably due to their smaller size.

The transitions of the binary bed between the segregated and mixed states are analyzed in terms of both spatial (penetration depth) and temporal (mixing and segregation times) scales. The results show that the mixing and segregating times are only moderately impacted by the varied experimental conditions. Higher fluidization velocities and taller beds promote faster transition from segregated to mixed states and vice versa. This behavior likely arises from enhanced bubble dynamics and flow patterns promoting rapid particle redistribution, while residual bubbles and bed voidage facilitate segregation.

CRediT authorship contribution statement

Azka Rizwana Siddiqui: Methodology, Investigation, Formal analysis, Data curation, Conceptualization, Writing – original draft. **Anna Köhler:** Supervision, Methodology, Conceptualization, Writing – review & editing. **Diana Carolina Guío-Pérez:** Supervision, Methodology, Conceptualization, Writing – review & editing. **David Pallarès:** Supervision, Methodology, Funding acquisition, Conceptualization, Writing – review & editing.

Declaration of competing interest

The authors declare the following financial interests/personal relationships which may be considered as potential competing interests:

David Pallares reports financial support was provided by Swedish Energy Agency. If there are other authors, they declare that they have no known competing financial interests or personal relationships that could have appeared to influence the work reported in this paper.

Acknowledgment

This research was supported by the Swedish Energy Agency through the project *Large-scale production of biocarbon as renewable feedstock in fossil-free value chains within the iron and steel industry* (P2022-00212). The authors would also like to thank Jakob Blomgren (Research Institutes of Sweden, RISE) for his contribution to the design and development of the magnetic solids tracing (MST) pin and the associated data acquisition system used in this study.

Appendix A

Impedance measurements are converted into concentrations of the lean solids phase by means of individual calibration curves. Such (Fig. A.1) curves are created based on measurements performed on mixtures of known concentrations. Error bars represent the standard deviation across repeated measurements for each mixture. The calibration mixtures consisted of magnetic powder and bronze powder. Bronze, with a density of 8492 kg/m^3 and mean particle size of 126 μm, served as a non-magnetic reference, while the magnetic powder has a density of 7988 kg/m^3 and mean particle size of 102 μm. Bronze was selected due to its similar properties, attempting to achieve homogeneous composition of mixture. The mixtures were first fluidizing in a small cylindrical fluidized bed (0.08 m I·D and $H_{bed} = 0.16$ m) with the MST pin inserted. The diameter of the cylindrical bed is larger than the circumference reached by the magnetic field of the sensing coil. After fluidizing the mixture for 2 min, fluidization was abruptly cut off, and impedance measurements were recorded. This was repeated three times, fluidizing between measurements to ensure homogenous distribution of the magnetic particles. The resulting calibration curves correlate known volumetric concentration of the magnetic powder to the measured impedance.

The lean solids phase was prepared by doping polymer clay with known amounts of the same magnetic powder. The magnetic powder concentration was converted to an equivalent lean solids concentration using a volumetric scaling factor of 12.4. This factor corresponds to the ratio $\frac{\text{Volume of Lean Solids}}{\text{Volume of Magnetic Powder}}$ and was determined from the known composition of the lean solids phase.

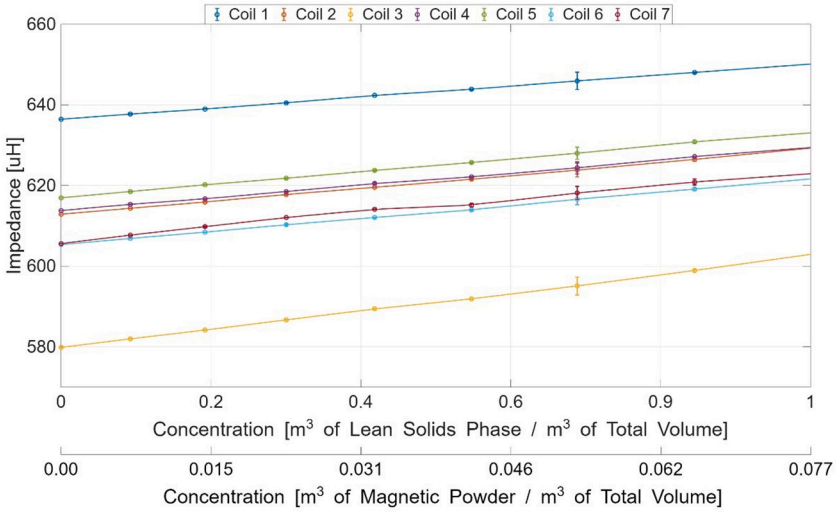

Fig. A.1. Calibration curves for the seven magnetic solid tracing coils embedded in the probe pin.

Appendix B

Appendix B presents a comparison of the bed expansion behaviors and the corresponding expanded bed heights for different fluidization velocities and static bed heights for unary beds (i.e., without the lean solids phase).

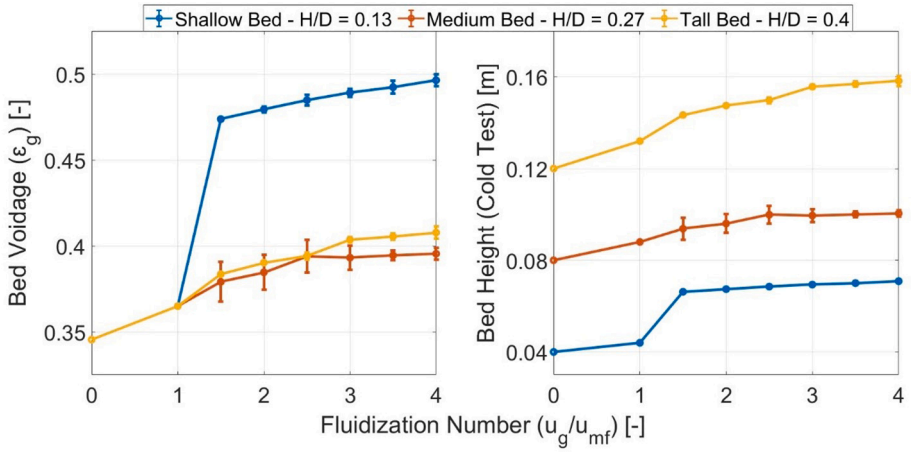

Fig. B.1. a) Mean bed voidage as a function of fluidization number for varying bed heights. b) Expanded bed heights for different fluidization velocities.

Appendix C

Appendix C presents the vertical distribution profiles corresponding to the cases discussed in Sections 3.2.2 and 3.2.3, under two fluidization conditions: low and high fluidization velocities. Mass conservation for each case is detailed in Table 3.

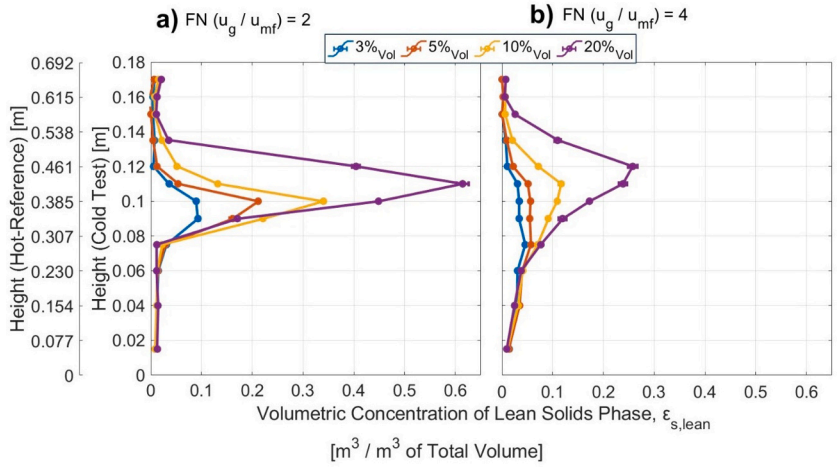

Fig. C.1. Vertical distribution profiles of the lean solids phase across varying loadings of the lean solids phase at a static bed height of $H_{b,0} = 0.08$ m (0.3 m). a) $u_g/u_{mf} = 2$; and b) $u_g/u_{mf} = 4$.

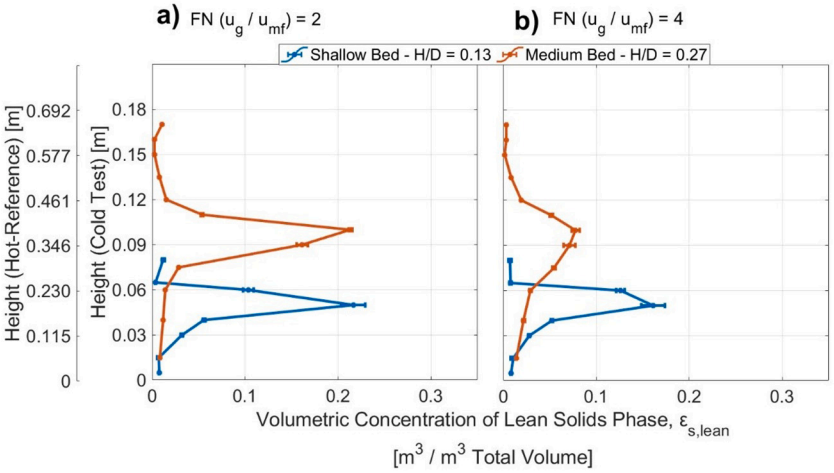

Fig. C.2. Vertical concentration profiles of the lean solids phase for varying static bed heights for a constant mass loading of $m_{lean} = 0.62$ kg. a) $u_g/u_{mf} = 2$; and b) $u_g/u_{mf} = 4$.

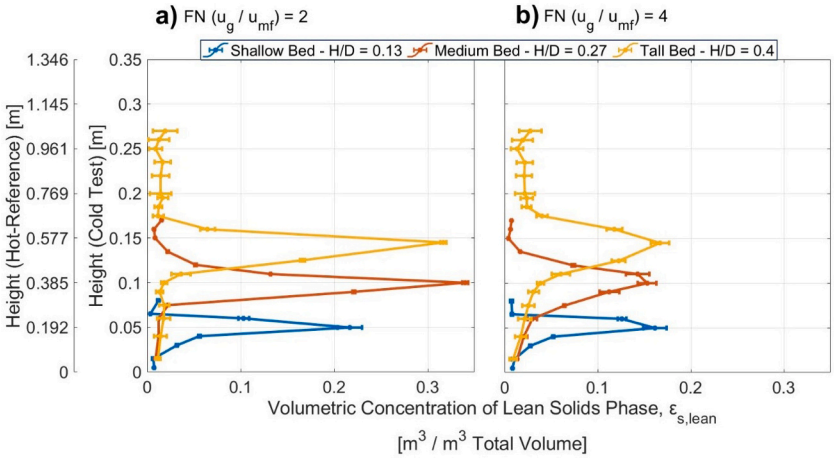

Fig. C.3. Vertical distribution profiles of the lean solids phase for varying static bed heights at a constant loading of $\varkappa_{lean} = 10\%_{vol}$. a) $u_g/u_{mf} = 2$; and b) $u_g/u_{mf} = 4$.

Data availability

Data will be made available on request.

References

[1] L. Shen, M. Zhang, Y. Xu, Solids mixing in fluidized beds, Powder Technol. 84 (1995) 207–212, https://doi.org/10.1016/0032-5910(95)02994-D.
[2] P.N. Rowe, P. Ba, A.G. Cheney, G.A. Henwood, E. Lyall, Mechanisms of solids mixing in fluidised beds, Trans. Inst. Chem. Eng. Chem. Eng. 43 (1965) T271.
[3] D. Kunii, O. Levenspiel, Fluidization Engineering, Elsevier, 2013.
[4] L.R. Glicksman, T. Yule, Prediction of the particle flow conditions in the freeboard of a freely bubbling fluidized bed, Chem. Eng. Sci. 50 (1995) 69–79, https://doi.org/10.1016/0009-2509(94)00208-9.
[5] M. Wirsum, F. Fett, N. Iwanowa, G. LGBRjanow, Particle mixing in bubbling fluidized beds of binary particle systems, Powder Technol. 120 (2001) 63–69, https://doi.org/10.1016/S0032-5910(01)00348-5.
[6] G. Olivieri, A. Marzocchella, P. Salatino, Segregation of fluidized binary mixtures of granular solids, AICHE J. 50 (2004) 3095–3106, https://doi.org/10.1002/aic.10340.
[7] Y. Zhang, B. Jin, W. Zhong, Experimental investigation on mixing and segregation behavior of biomass particle in fluidized bed, Chem. Eng. Process. Process Intensif. 48 (2009) 745–754, https://doi.org/10.1016/j.cep.2008.09.004.
[8] H.T. Jang, T.S. Park, W.S. Cha, Mixing-segregation phenomena of binary system in a fluidized bed, J. Ind. Eng. Chem. 16 (2010) 390–394, https://doi.org/10.1016/j.jiec.2009.10.003.
[9] K.V.N.S. Rao, G.V. Reddy, Cold flow studies of rice husk, saw dust, and groundnut shell fuels in a fluidized bed, Energy Sources, Part A Recover. Util. Environ. Eff. 32 (2010) 1701–1711, https://doi.org/10.1080/15567030902882893.
[10] R.K. Upadhyay, S. Roy, Investigation of hydrodynamics of binary fluidized beds via radioactive particle tracking and dual-source densitometry, Can. J. Chem. Eng. 88 (2010) 601–610, https://doi.org/10.1002/cjce.20334.
[11] J. Halow, K. Holsopple, B. Crawshaw, S. Daw, C. Finney, Observed mixing behavior of single particles in a bubbling fluidized bed of higher-density particles, Ind. Eng. Chem. Res. 51 (2012) 14566–14576, https://doi.org/10.1021/ie301517w.
[12] K. Zhang, B. Yu, J. Chang, G. Wu, T. Wang, D. Wen, Hydrodynamics of a fluidized bed co-combustor for tobacco waste and coal, Bioresour. Technol. 119 (2012) 339–348, https://doi.org/10.1016/j.biortech.2012.05.132.
[13] O.O. Olaofe, K.A. Buist, N.G. Deen, M.A. van der Hoef, J.A.M. Kuipers, Segregation dynamics in dense polydisperse gas-fluidized beds, Powder Technol. 246 (2013) 695–706, https://doi.org/10.1016/j.powtec.2013.05.047.
[14] B. Cluet, G. Mauviel, Y. Rogaume, O. Authier, A. Delebarre, Segregation of wood particles in a bubbling fluidized bed, Fuel Process. Technol. 133 (2015) 80–88, https://doi.org/10.1016/j.fuproc.2014.12.045.
[15] F. Fotovat, R. Ansart, M. Hemati, O. Simonin, J. Chaouki, Sand-assisted fluidization of large cylindrical and spherical biomass particles: experiments and simulation, Chem. Eng. Sci. 126 (2015) 543–559, https://doi.org/10.1016/j.ces.2014.12.022.
[16] A. Köhler, A. Rasch, D. Pallarès, F. Johnsson, Experimental characterization of axial fuel mixing in fluidized beds by magnetic particle tracking, Powder Technol. 316 (2017) 492–499, https://doi.org/10.1016/j.powtec.2016.12.093.
[17] P. Brachi, R. Chirone, F. Miccio, M. Miccio, G. Ruoppolo, Segregation and fluidization behavior of poly-disperse mixtures of biomass and inert particles, Chem. Eng. Trans. 57 (2017) 811–816, https://doi.org/10.3303/CET1757136.
[18] J. Huang, Y. Lu, H. Wang, A new quantitative measurement method for mixing and segregation of binary-mixture fluidized bed by capacitance probe, Chem. Eng. J. 326 (2017) 99–108, https://doi.org/10.1016/j.cej.2017.05.126.
[19] B.K. Singh, S. Roy, V.V. Buwa, Dynamics of segregation and fluidization of binary mixtures in a cylindrical fluidized bed, AICHE J. 65 (2019) 1–15, https://doi.org/10.1002/aic.16682.
[20] S. Parvathaneni, V.V. Buwa, Role of bubbling behaviour in segregation and mixing of binary gas-solids flow of particles with different density, Powder Technol. 372 (2020) 178–191, https://doi.org/10.1016/j.powtec.2020.05.072.
[21] C.R.K. Windows-Yule, A. Moore, C. Wellard, D. Werner, D.J. Parker, J.P.K. Seville, Particle distributions in binary gas-fluidised beds: shape matters – but not much, Chem. Eng. Sci. 216 (2020) 115440, https://doi.org/10.1016/j.ces.2019.115440.
[22] C.R.K. Windows-Yule, S. Gibson, D. Werner, D.J. Parker, T.Z. Kokalova, J.P. K. Seville, Effect of distributor design on particle distribution in a binary fluidised bed, Powder Technol. 367 (2020) 1–9, https://doi.org/10.1016/j.powtec.2020.03.034.
[23] J. Huang, K. Dong, M. Lv, H. Li, Z. Liu, Comprehensive study on the mixing behavior of small dissimilar particles in a fluidized bed, Ind. Eng. Chem. Res. 59 (2020) 21982–21993, https://doi.org/10.1021/acs.iecr.0c04603.
[24] T. Emiola-Sadiq, J. Wang, L. Zhang, A. Dalai, Mixing and segregation of binary mixtures of biomass and silica sand in a fluidized bed, Particuology 58 (2021) 58–73, https://doi.org/10.1016/j.partic.2021.01.010.
[25] S. Roy, H.J. Pant, S. Roy, Velocity characterization of solids in binary fluidized beds, Chem. Eng. Sci. 246 (2021) 116883, https://doi.org/10.1016/j.ces.2021.116883.
[26] Y. Li, L. Du, Y. Zhao, Z. Wang, F. Zhu, Z. Lu, C. Duan, L. Dong, C. Zhou, Segregation and mixing behavior of geldart d binary particles in pulsed gas-solid fluidized bed, Part. Sci. Technol. 40 (2022) 434–444, https://doi.org/10.1080/02726351.2021.1954116.
[27] V. Del Duca, P. Brachi, R. Chirone, R. Chirone, A. Coppola, M. Miccio, G. Ruoppolo, Binary mixtures of biomass and inert components in fluidized beds: experimental and neural network exploration, Fuel 346 (2023) 128314, https://doi.org/10.1016/j.fuel.2023.128314.
[28] D. Werner, H. Davison, E. Robinson, J.A. Sykes, J.P.K. Seville, A. Wellings, S. Bhattacharya, D.A. Sanchez Monsalve, T. Kokalova Wheldon, C.R.K. Windows-Yule, Effect of system composition on mixing in binary fluidised beds, Chem. Eng. Sci. 271 (2023) 118562, https://doi.org/10.1016/j.ces.2023.118562.
[29] L. Molignano, M. Troiano, R. Solimene, S. Tebianian, J.-F. Joly, P. Salatino, Investigation of mixing/segregation patterns of two dissimilar granular solids in fluidized beds by capacitance probes, Chem. Eng. Sci. 322 (2026) 123047, https://doi.org/10.1016/j.ces.2025.123047.
[30] T. Berdugo Vilches, H. Thunman, Experimental investigation of volatiles-bed contact in a 2-4 MWth bubbling bed reactor of a dual fluidized bed gasifier, Energy Fuel 29 (2015) 6456–6464, https://doi.org/10.1021/acs.energyfuels.5b01303.
[31] E. Sette, T. Berdugo Vilches, D. Pallarès, F. Johnsson, Measuring fuel mixing under industrial fluidized-bed conditions - a camera-probe based fuel tracking system, Appl. Energy 163 (2016) 304–312, https://doi.org/10.1016/j.apenergy.2015.11.024.
[32] A.T. Harris, J.F. Davidson, R.B. Thorpe, Particle residence time distributions in circulating fluidised beds, Chem. Eng. Sci. 58 (2003) 2181–2202, https://doi.org/10.1016/S0009-2509(03)00082-4.
[33] I.N.S. Winaya, T. Shimizu, D. Yamada, A new method to evaluate horizontal solid dispersion in a bubbling fluidized bed, Powder Technol. 178 (2007) 173–178, https://doi.org/10.1016/j.powtec.2007.05.005.
[34] C. Yan, Y. Fan, C. Lu, Y. Zhang, Y. Liu, R. Cao, J. Gao, C. Xu, Solids mixing in a fluidized bed riser, Powder Technol. 193 (2009) 110–119, https://doi.org/10.1016/j.powtec.2009.02.015.
[35] T. Fitzgerald, N. Catipovic, G. Jovanovic, C. Bliss, B. Williams, Solid tracer studies in a tube-filled fluidized bed, Circ. Fluid. Bed Combust. 5 (1977) 135–152.
[36] A. Avidan, J. Yerushalmi, Solids mixing in an expanded top fluid bed, AICHE J. 31 (1985) 835–841, https://doi.org/10.1002/aic.690310520.
[37] D.C. Guío-Pérez, T. Pröll, H. Hofbauer, Measurement of ferromagnetic particle concentration for characterization of fluidized bed fluid-dynamics, Powder Technol. 239 (2013) 147–154, https://doi.org/10.1016/j.powtec.2013.01.040.
[38] D.C. Guío-Pérez, F. Dietrich, J.N. Ferreira Cala, T. Pröll, H. Hofbauer, Estimation of solids circulation rate through magnetic tracer tests, Powder Technol. 316 (2017) 650–657, https://doi.org/10.1016/j.powtec.2017.04.062.
[39] M. Farha, D.C. Guío-Pérez, J. Aronsson, F. Johnsson, D. Pallarès, Assessment of experimental methods for measurements of the horizontal flow of fluidized solids under bubbling conditions, Fuel 348 (2023), https://doi.org/10.1016/j.fuel.2023.128515.
[40] M. Farha, D.C. Guío-Pérez, F. Johnsson, D. Pallarès, Characterization of the solids crossflow in a bubbling fluidized bed, Powder Technol. 443 (2024), https://doi.org/10.1016/j.powtec.2024.119967.
[41] N. Nemati, T. Pröll, T. Mattisson, M. Rydén, Impact of random packing on residence time distribution of particles in bubbling fluidized beds: part 1–cross-current flow reactors, Chem. Eng. Sci. 302 (2025), https://doi.org/10.1016/j.ces.2024.120724.
[42] N. Nemati, T. Mattisson, D. Pallarès, D.C. Guío-Pérez, M. Rydén, Impact of random packing on residence time distribution of particles in bubbling fluidized beds: part 2 - counter-current flow reactors, Powder Technol. 465 (2025), https://doi.org/10.1016/j.powtec.2025.121306.
[43] R. Girimonte, B. Formisani, The minimum bubbling velocity of fluidized beds operating at high temperature, Powder Technol. 189 (2009) 74–81, https://doi.org/10.1016/j.powtec.2008.06.006.
[44] W.R.A. Goossens, Classification of fluidized particles by archimedes number, Powder Technol. 98 (1998) 48–53, https://doi.org/10.1016/S0032-5910(98)00027-8.
[45] M.T. Nicastro, L.R. Glicksman, Experimental verification of scaling relationships for fluidized bed, Chem. Eng. Sci. 39 (1984) 1381–1391, https://doi.org/10.1016/0009-2509(84)80071-8.
[46] L.R. Glicksman, Scaling relationships for fluidized beds, Chem. Eng. Sci. 39 (1984) 1373–1379, https://doi.org/10.1016/0009-2509(84)80070-6.
[47] L.R. Glicksman, M.R. Hyre, P.A. Farrell, Dynamic similarity in fluidization, Int. J. Multiphase Flow 20 (1994) 331–386, https://doi.org/10.1016/0301-9322(94)90077-9.
[48] T. Fitzgerald, D. Bushnell, S. Crane, Y.C. Shieh, Testing of cold scaled bed modeling for fluidized-bed combustors, Powder Technol. 38 (1984) 107–120, https://doi.org/10.1016/0032-5910(84)80040-6.
[49] M. Stein, Y.L. Ding, J.P.K. Seville, Experimental verification of the scaling relationships for bubbling gas-fluidised beds using the PEPT technique, Chem. Eng. Sci. 57 (2002) 3649–3658, https://doi.org/10.1016/S0009-2509(02)00264-6.
[50] E. Sette, D. Pallarès, F. Johnsson, Experimental quantification of lateral mixing of fuels in fluid-dynamically down-scaled bubbling fluidized beds, Appl. Energy 136 (2014) 671–681, https://doi.org/10.1016/j.apenergy.2014.09.075.
[51] B. Leckner, P. Szentannai, F. Winter, Scale-up of fluidized-bed combustion-a review, Fuel 90 (2011) 2951–2964, https://doi.org/10.1016/j.fuel.2011.04.038.
[52] C.M. van den Bleek, J.C. Schouten, Deterministic chaos: a new tool in fluidized bed design and operation, Chem. Eng. J. Biochem. Eng. J. 53 (1993) 75–87, https://doi.org/10.1016/0923-0467(93)80009-L.
[53] C.M. Van Den Bleek, J.C. Schouten, Can deterministic chaos create order in fluidized-bed scale-up? Chem. Eng. Sci. 48 (1993) 2367–2373, https://doi.org/10.1016/0009-2509(93)81058-4.
[54] C.M. van den Bleek, M.-O. Coppens, J.C. Schouten, Application of chaos analysis to multiphase reactors, Chem. Eng. Sci. 57 (2002) 4763–4778, https://doi.org/10.1016/S0009-2509(02)00288-9.

[55] L. Kalo, H.J. Pant, M.C. Cassanello, R.K. Upadhyay, Time series analysis of a binary gas-solid conical fluidized bed using radioactive particle tracking (RPT) technique data, Chem. Eng. J. 377 (2019) 119807, https://doi.org/10.1016/j.cej.2018.08.193.
[56] J. Gao, X. Lan, Y. Fan, J. Chang, G. Wang, C. Lu, C. Xu, Hydrodynamics of gas – solid fluidized bed of disparately sized binary particles, Chem. Eng. Sci. 64 (2009) 4302–4316, https://doi.org/10.1016/j.ces.2009.07.003.
[57] Q. Gou, D. Song, H. Wu, S. Wen, G. Chen, Effect of mixing ratio on flow characteristics of binary particles in a fluidized bed, Powder Technol. 462 (2025) 121132, https://doi.org/10.1016/j.powtec.2025.121132.
[58] B. Anicic, B. Lu, W. Lin, H. Wu, K. Dam-Johansen, W. Wang, CFD simulation of mixing and segregation of binary solid mixtures in a dense fluidized bed, Can. J. Chem. Eng. 98 (2020) 412–420, https://doi.org/10.1002/cjce.23561.
[59] H. Ma, Y. Zhao, CFD-DEM investigation of the fluidization of binary mixtures containing rod-like particles and spherical particles in a fluidized bed, Powder Technol. 336 (2018) 533–545, https://doi.org/10.1016/j.powtec.2018.06.034.
[60] H. Wang, Z. Zhong, A mixing behavior study of biomass particles and sands in fluidized bed based on CFD-DEM simulation, Energies 12 (2019), https://doi.org/10.3390/en12091801.
[61] Y. Yu, F. Lu, X. He, F. Wei, C. Zhang, Segregation of binary particles in gas-solid fluidized bed, Front. Chem. Sci. Eng. 18 (2024) 1–9, https://doi.org/10.1007/s11705-024-2426-0.
[62] A. Köhler, D.C. Guío-Pérez, A. Prati, M. Larcher, D. Pallarès, Rheological effects of a gas fluidized bed emulsion on falling and rising spheres, Powder Technol. 393 (2021) 510–518, https://doi.org/10.1016/j.powtec.2021.07.064.
[63] A.M. Gomez, M. Nikku, P. Jalali, Direct measurement of solid drag force in fluid–particle flow, WIT Trans. Eng. Sci. 123 (2019) 11–20, https://doi.org/10.2495/MPF190021.
[64] M. Farzaneh, S. Sasic, A.E. Almstedt, F. Johnsson, D. Pallarès, A study of fuel particle movement in fluidized beds, Ind. Eng. Chem. Res. 52 (2013) 5791–5805, https://doi.org/10.1021/ie301515v.
[65] M. Nikku, K. Myöhänen, J. Ritvanen, T. Hyppänen, M. Lyytikäinen, Three-dimensional modeling of biomass fuel flow in a circulating fluidized bed furnace with an experimentally derived momentum exchange model, Chem. Eng. Res. Des. 115 (2016) 77–90, https://doi.org/10.1016/j.cherd.2016.09.023.
[66] A. Köhler, D. Pallarès, F. Johnsson, Modeling axial mixing of fuel particles in the dense region of a fluidized bed, Energy Fuel 34 (2020) 3294–3304, https://doi.org/10.1021/acs.energyfuels.9b04194.
[67] J.R. Grace, F. Taghipour, Verification and validation of CFD models and dynamic similarity for fluidized beds, Powder Technol. 139 (2004) 99–110, https://doi.org/10.1016/j.powtec.2003.10.006.
[68] C.K. Jayarathna, M. Balfe, B.E. Moldestad, L.A. Tokheim, Comparison of experimental results from operating a novel fluidized bed classifier with CFD simulations applying different drag models and model validation †, Processes 10 (2022) https://doi.org/10.3390/pr10091855.
[69] J.P. Couderc, Incipient fluidization and particulate systems, in: J.F. Davidson, R. Clift, D. Harrison (Eds.), Fluidization, Second Edi, Academic Press, 1985, pp. 1–44.
[70] A.A. Avidan, J. Yerushalmi, Bed expansion in high velocity fluidization, Powder Technol. 32 (1982) 223–232, https://doi.org/10.1016/0032-5910(82)85024-9.
[71] F. Johnsson, S. Andersson, B. Leckner, Expansion of a freely bubbling fluidized bed, Powder Technol. 68 (1991) 117–123, https://doi.org/10.1016/0032-5910(91)80118-3.
[72] W. Jin, J. Gao, C. E, Y. Fan, C. Lu, Pressure fluctuations in a fluidized bed of binary particles with significant differences in particle size, Chem. Eng. Sci. 287 (2024) 119704, https://doi.org/10.1016/j.ces.2024.119704.
[73] A. Soria-Verdugo, L.M. Garcia-Gutierrez, S. Sanchez-Delgado, U. Ruiz-Rivas, Circulation of an object immersed in a bubbling fluidized bed, Chem. Eng. Sci. 66 (2011) 78–87, https://doi.org/10.1016/j.ces.2010.10.006.
[74] A. Soria-Verdugo, L.M. Garcia-Gutierrez, N. García-Hernando, U. Ruiz-Rivas, Buoyancy effects on objects moving in a bubbling fluidized bed, Chem. Eng. Sci. 66 (2011) 2833–2841, https://doi.org/10.1016/j.ces.2011.03.055.
[75] P.N. Rowe, B.A. Partridge, An x-ray study of bubbles in fluidised beds, Chem. Eng. Res. Des. 75 (1997) S116–S134, https://doi.org/10.1016/S0263-8762(97)80009-3.
[76] G.M. Rios, K.D. Tran, H. Masson, Free object motion in a gas fluidized bed, Chem. Eng. Commun. 47 (1986) 247–272, https://doi.org/10.1080/00986448608911767.
[77] A.W. Nienow, T. Chiba, Fluidization of dissimilar materials, in: J.F. Davidson, R. Clift, D. Harrison (Eds.), Fluidization, Second Edi, Academic Press, 1985, pp. 357–382.
[78] S.Y. Wu, J. Baeyens, Segregation by size difference in gas fluidized beds, Powder Technol. 98 (1998) 139–150, https://doi.org/10.1016/S0032-5910(98)00026-6.
[79] N. Mostoufi, J. Chaouki, Local solid mixing in gas-solid fluidized beds, Powder Technol. 114 (2001) 23–31, https://doi.org/10.1016/S0032-5910(00)00258-8.
[80] J.F. Brainovich, MixingEegregation in Two- and Three-Dimensional Fluidized Beds : Binary Systems of Equidensity Spherical Particles 32, 1986, pp. 7–16.
[81] S.R. Dahl, C.M. Hrenya, Size segregation in gas – solid fluidized beds with continuous size distributions, Chem. Eng. Sci. 60 (2005) 6658–6673, https://doi.org/10.1016/j.ces.2005.05.057.
[82] Z. Amiri, S. Movahedirad, M. Shirvani, Particles Mixing Induced by Bubbles in a Gas-Solid Fluidized Bed, 2016, p. 62, https://doi.org/10.1002/aic.15150.
[83] O.A. Jaiboon, B. Chalermsinsuwan, L. Mekasut, P. Piumsomboon, Effect of flow pattern on power spectral density of pressure fluctuation in various fluidization regimes, Powder Technol. 233 (2013) 215–226, https://doi.org/10.1016/j.powtec.2012.09.014.
[84] F. Johnsson, R.C. Zijerveld, J.C. Schouten, C.M. Van Den Bleek, B. Leckner, Characterization of fluidization regimes by time-series analysis of pressure fluctuations, Int. J. Multiphase Flow 26 (2000) 663–715, https://doi.org/10.1016/S0301-9322(99)00028-2.
[85] A. Svensson, F. Johnsson, B. Leckner, Bottom bed regimes in a circulating fluidized bed boiler, Int. J. Multiphase Flow 22 (1996) 1187–1204, https://doi.org/10.1016/0301-9322(96)00025-0.